MIT Libraries | DSpace@MIT

MIT Open Access Articles

Multi-omic analysis in injured humans: Patterns align with outcomes and treatment responses

The MIT Faculty has made this article openly available. ***Please share*** how this access benefits you. Your story matters.

Citation: Wu, Junru, Vodovotz, Yoram, Abdelhamid, Sultan, Guyette, Francis X, Yaffe, Michael B et al. 2021. "Multi-omic analysis in injured humans: Patterns align with outcomes and treatment responses." Cell Reports Medicine, 2 (12).

As Published: 10.1016/J.XCRM.2021.100478

Publisher: Elsevier BV

Persistent URL: https://hdl.handle.net/1721.1/147022

Version: Final published version: final published article, as it appeared in a journal, conference proceedings, or other formally published context

Terms of use: Creative Commons Attribution-NonCommercial-NoDerivs License

Massachusetts Institute of Technology

Cell Reports
Medicine

Article

Multi-omic analysis in injured humans: Patterns align with outcomes and treatment responses

Graphical abstract

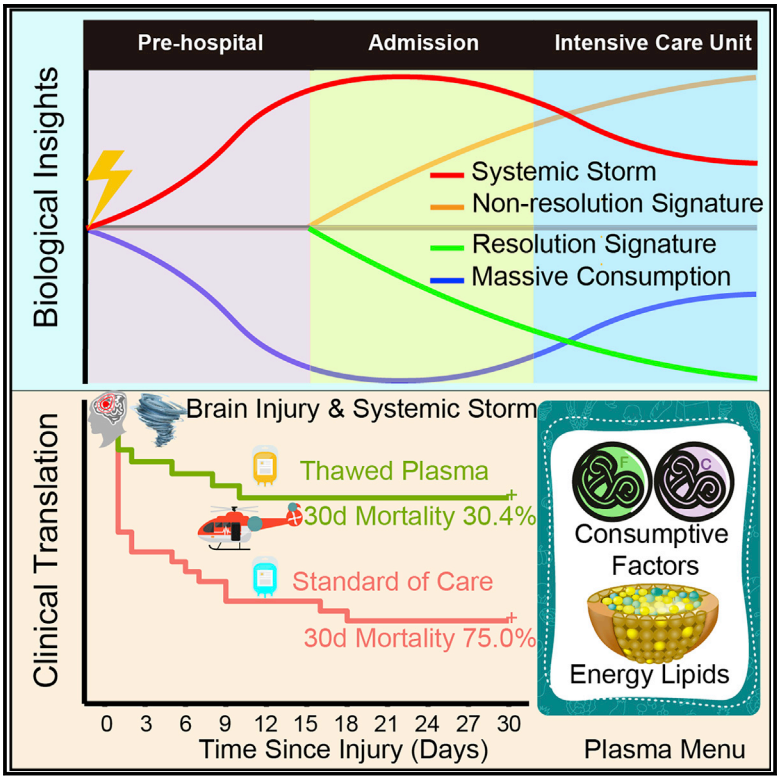

Highlights

- An integrated longitudinal multi-omic analysis of the human response to trauma
- Systemic storm and massive consumption patterns are related to early mortality
- Unique resolution and non-resolution signatures across multiple "omics" platforms
- Only endotype 2-TBI patients with high UCHL1 levels benefit from early plasma

Authors

Junru Wu, Yoram Vodovotz, Sultan Abdelhamid, ..., Jason L. Sperry, Timothy R. Billiar, PAMPer study group

Correspondence

nealm2@upmc.edu (M.D.N.), sperryjl@upmc.edu (J.L.S.), billiartr@upmc.edu (T.R.B.)

In brief

Wu et al. report a longitudinal multi-omic analysis of the circulation in trauma patients. Cross-platform data integration reveals a massive systemic release of cellular contents ("systemic storm") and simultaneous consumption of blood constituents. Also defined are patient endotypes that differ in outcomes and responses to early plasma administration.

Wu et al., 2021, Cell Reports Medicine 2, 100478
December 21, 2021
https://doi.org/10.1016/j.xcrm.2021.100478

CellPress

Cell Reports Medicine

CellPress
OPEN ACCESS

Article

Multi-omic analysis in injured humans: Patterns align with outcomes and treatment responses

Junru Wu,[1,2,3,4] Yoram Vodovotz,[1,2] Sultan Abdelhamid,[1,2] Francis X. Guyette,[5] Michael B. Yaffe,[6,7] Danielle S. Gruen,[1,2] Anthony Cyr,[1,2] David O. Okonkwo,[8] Upendra K. Kar,[1,2] Neha Krishnamoorthi,[1] Robert G. Voinchet,[1] Isabel M. Billiar,[1] Mark H. Yazer,[9] Rami A. Namas,[1,2] Brian J. Daley,[10] Richard S. Miller,[11] Brian G. Harbrecht,[12] Jeffrey A. Claridge,[13] Herbert A. Phelan,[14] Brian S. Zuckerbraun,[1,2] Pär I. Johansson,[15] Jakob Stensballe,[15,16,17] James H. Morrissey,[18] Russell P. Tracy,[19] Stephen R. Wisniewski,[20] Matthew D. Neal,[1,2,*] Jason L. Sperry,[1,2,*] Timothy R. Billiar,[1,2,22,*] and PAMPer study group,[21]

[1]Department of Surgery, University of Pittsburgh, Pittsburgh, PA, USA
[2]Pittsburgh Trauma Research Center, University of Pittsburgh, Pittsburgh, PA, USA
[3]Department of Cardiology & Center of Pharmacology, The 3rd Xiangya Hospital, Central South University, Changsha, China
[4]Eight-Year Program of Medicine, Xiangya School of Medicine, Central South University, Changsha, China
[5]Department of Emergency Medicine, Medicine, University of Pittsburgh, Pittsburgh, PA, USA
[6]Koch Institute for Integrative Cancer Research, Massachusetts Institute of Technology, Cambridge, MA, USA
[7]Department of Surgery, Beth Israel Deaconess Medical Center, Harvard Medical School, Boston, MA, USA
[8]Department of Neurological Surgery, University of Pittsburgh, Pittsburgh, PA, USA
[9]The Institute for Transfusion Medicine, Pittsburgh, PA, USA
[10]Department of Surgery, University of Tennessee Health Science Center, Knoxville, TN, USA
[11]Department of Surgery, JPS Health Network in Fort Worth, TX, USA
[12]Department of Surgery, University of Louisville, Louisville, KY, USA
[13]Metro Health Medical Center, Case Western Reserve University, Cleveland, OH, USA
[14]Department of Surgery, University of Texas Southwestern, Dallas, TX, USA
[15]Section for Transfusion Medicine, Capital Region Blood Bank, Rigshospitalet, Copenhagen University Hospital, Copenhagen, Denmark
[16]Department of Anesthesia and Trauma Center, Centre of Head and Orthopaedics, Rigshospitalet, Copenhagen University Hospital, Copenhagen, Denmark
[17]Emergency Medical Services, The Capital Region of Denmark, Hillerød, Denmark
[18]Departments of Biological Chemistry & Internal Medicine, University of Michigan Medical School, Ann Arbor, MI, USA
[19]Department of Pathology & Laboratory Medicine and Biochemistry, University of Vermont Larner College of Medicine, Colchester, VT, USA
[20]Graduate School of Public Health, University of Pittsburgh, Pittsburgh, PA, USA
[21]The PAMPer study group is detailed in Supplemental acknowledgments (Document S1)
[22]Lead contact
*Correspondence: nealm2@upmc.edu (M.D.N.), sperryjl@upmc.edu (J.L.S.), billiartr@upmc.edu (T.R.B.)
https://doi.org/10.1016/j.xcrm.2021.100478

SUMMARY

Trauma is a leading cause of death and morbidity worldwide. Here, we present the analysis of a longitudinal multi-omic dataset comprising clinical, cytokine, endotheliopathy biomarker, lipidome, metabolome, and proteome data from severely injured humans. A "systemic storm" pattern with release of 1,061 markers, together with a pattern suggestive of the "massive consumption" of 892 constitutive circulating markers, is identified in the acute phase post-trauma. Data integration reveals two human injury response endotypes, which align with clinical trajectory. Prehospital thawed plasma rescues only endotype 2 patients with traumatic brain injury (30-day mortality: 30.3 versus 75.0%; p = 0.0015). Ubiquitin carboxy-terminal hydrolase L1 (UCHL1) was identified as the most predictive circulating biomarker to identify endotype 2-traumatic brain injury (TBI) patients. These response patterns refine the paradigm for human injury, while the datasets provide a resource for the study of critical illness, trauma, and human stress responses.

INTRODUCTION

Trauma is a common cause of preventable death and the leading etiology of death and disability in humans under age 55, resulting in a huge global health burden.[1] The current paradigms used to explain the adaptive and pathologic host responses to severe injury are the result of more than a century of studies of injured humans as well as model organisms, tissues, and cells.[2] This has yielded insights into organ- and system-specific features of the consequences of severe injury, including neurohumoral abnormalities,[3] endotheliopathy and coagulopathy,[4,5] hypermetabolism and acidosis,[6] systemic hyper-inflammation and genomic storm,[7,8] and multi-organ dysfunction.[9] It has become clear that similarly injured humans can follow very different

This is an open access article under the CC BY-NC-ND license (http://creativecommons.org/licenses/by-nc-nd/4.0/).

clinical trajectories and outcomes and that the nature of the host response can dictate outcomes.[10,11] However, the lack of a comprehensive and integrated picture of these response patterns remains among the most important impediments to progress in the field.

Multi-omic analysis of large patient populations as a so called "deep cohort" can create a more comprehensive view of human disease responses.[12] The application of cross-platform omics (e.g., genomics/transcriptomics/proteomics/metabolomics) at the bulk (tissue or body fluid) and single-cell levels has begun to provide insights into the central principles driving the pathogenesis of infection-related critical illnesses (i.e., sepsis, severe coronavirus disease 2019 [COVID-19]).[13–18] However, studies into infection-induced disease are challenged by the confounders of concomitant chronic diseases and an inability to pinpoint the time of onset.[19,20] The critical illness resulting from trauma frequently involves otherwise young, healthy individuals, and the time of onset of the inciting event is easily identified. These unique features make trauma an ideal condition to define events that take place during the dynamic evolution of humans from a healthy state to critical illness using multi-omic data integration strategies.

Here, we analyzed a six-layer multi-omics dataset of trauma patients that includes clinical, cytokine, endotheliopathy biomarkers (ECs), lipidome, metabolome, and proteome longitudinal information. The patients and plasma biobank were a subset of the Prehospital Air Medical Plasma (PAMPer) trial,[21] a prospective multi-center randomized efficacy study of prehospital allogeneic thawed plasma (TP) in injured humans transported to trauma centers by air ambulance. The results demonstrated that early TP administration significantly reduced 30-day mortality compared with standard care. The major goal for our study was to identify the potential key drivers of the early and late outcomes of severely injured, critically ill humans. We also leveraged the strong positive TP treatment effect to explore whether TP modulated any of the putative drivers to provide insights into the mechanisms of action of TP. The analysis and datasets provide an important resource for the study of critical illness, trauma, and human stress responses.

RESULTS

Summary of study design, cohort details, and layers

To explore the features of the human response to severe injury, we analyzed multi-omics datasets derived from two human trauma cohorts. The primary cohort was derived from the PAMPer trial,[21] and the second cohort was a validation dataset from a previously published cohort of 472 blunt trauma survivors (trauma dataset 2 [TD2]).[7] Metadata for both cohorts are shown in Figure 1. Six distinct data layers were available for analysis with longitudinal information shown by layer in Figure 1A. Data layers from PAMPer patients, included clinical data (n = 501), plasma ECs; n = 390), quantitative measurement of 21 circulating inflammatory mediators (cytokines; n = 393), quantitative lipidomics (n = 194), untargeted metabolomics (n = 194), and multiplexed proteomics (n = 156) (Figure 1B; Figure S1). The TD2 dataset was limited to clinical data (n = 472), cytokines (n = 472), and untargeted plasma metabolomics (n = 86) (Figure 1C). The distribution of patients by outcomes categorized as resolving (intensive care unit [ICU] length of stay < 7 days), non-resolving (ICU length of stay $\geq$ 7 days or death after 72 h), or early nonsurvivors (death < 72 h) across the data layers is shown in Figures 1B and 1C. The patient makeup by multi-omic datasets included either five data layers (n = 181) or six data layers (n = 97) for PAMPer and three data layers (n = 86) for TD2 (Figures 1B and 1C). There was also a broad distribution of three levels of injury severity based on the injury severity score (ISS 0–15, mild; ISS 16–25, moderate; ISS $\geq$ 25, severe) in all layers (Figures S2A and S2B). The 0 h time point indicates the time of admission to the emergency department, which was less than 1 h after injury for most patients (Figures S2C and S2D). Prehospital transfusion of packed red blood cells and crystalloid were comparable among all outcome groups (Figures S2C and S2D).

K-means clustering identifies seven distinct metabolite modules that associate with outcomes

The clinical data, EC, cytokines, and lipidomic data for PAMPer and all three layers for TD2 have been previously published.[21–24] Here, we provide an overview of the metabolomic and proteomic findings for the PAMPer cohort. Untargeted plasma metabolomics was performed on 17 non-fasting healthy controls (HCs) and 194 trauma patients at 0, 24, and 72 h after arrival to the hospital. The non-fasting subjects serve as controls primarily for the 0 h time point. The demographic information of all patients in the metabolome layer is shown in Table S1. A total of 899 metabolites were detected in the PAMPer dataset, and a similar distribution of metabolite classes was seen across both datasets (n = 660), with lipids, amino acids, and xenobiotics comprising the largest number (Figures S3A and S3B). There was excellent correlation for metabolites quantified as part of clinical blood assays (glucose, lactate, creatine, blood urea nitrogen [BUN], and bilirubin) and the measurements of these molecules in the metabolomics assay (Figure S3C).

To visualize global differences by outcome and across time, HC and patient-specific metabolomic profiles for the three time points were projected onto uniform manifold approximation and projection (UMAP) plots (Figure 2A).[25] HCs were tightly clustered and could be clearly distinguished from trauma patients. The area encircled by the red line on the UMAP plots identifies the time 0 h pattern associated with slow resolution or early death (Figures 2A and 2B). A distinct pattern was also observed at 24 and 72 h for non-resolving patients (encircled by the blue line). The metabolomic patterns were further resolved by K-means clustering, with k = 7 (Figure 2C; Figures S4A and S4B). These seven modules varied by both time and patient outcomes (Table S4). The general patterns from the resolving and the non-resolving outcomes were confirmed in the TD2 dataset (Figure 2D). Striking differences in the metabolite patterns were observed across modules. Module 1, which represented metabolites that were low in HCs and at time 0 h, were elevated at 24 h and to a much greater degree in non-resolving patients. Module 2, also low in HCs and time 0 h, increased in non-resolving patients at 72 h. Modules 3 and 4 were low in HCs, but showed a dramatic increase at time 0 h, especially in the patient groups with the worst outcomes. The increase in module 3 metabolites

CellPress
OPEN ACCESS

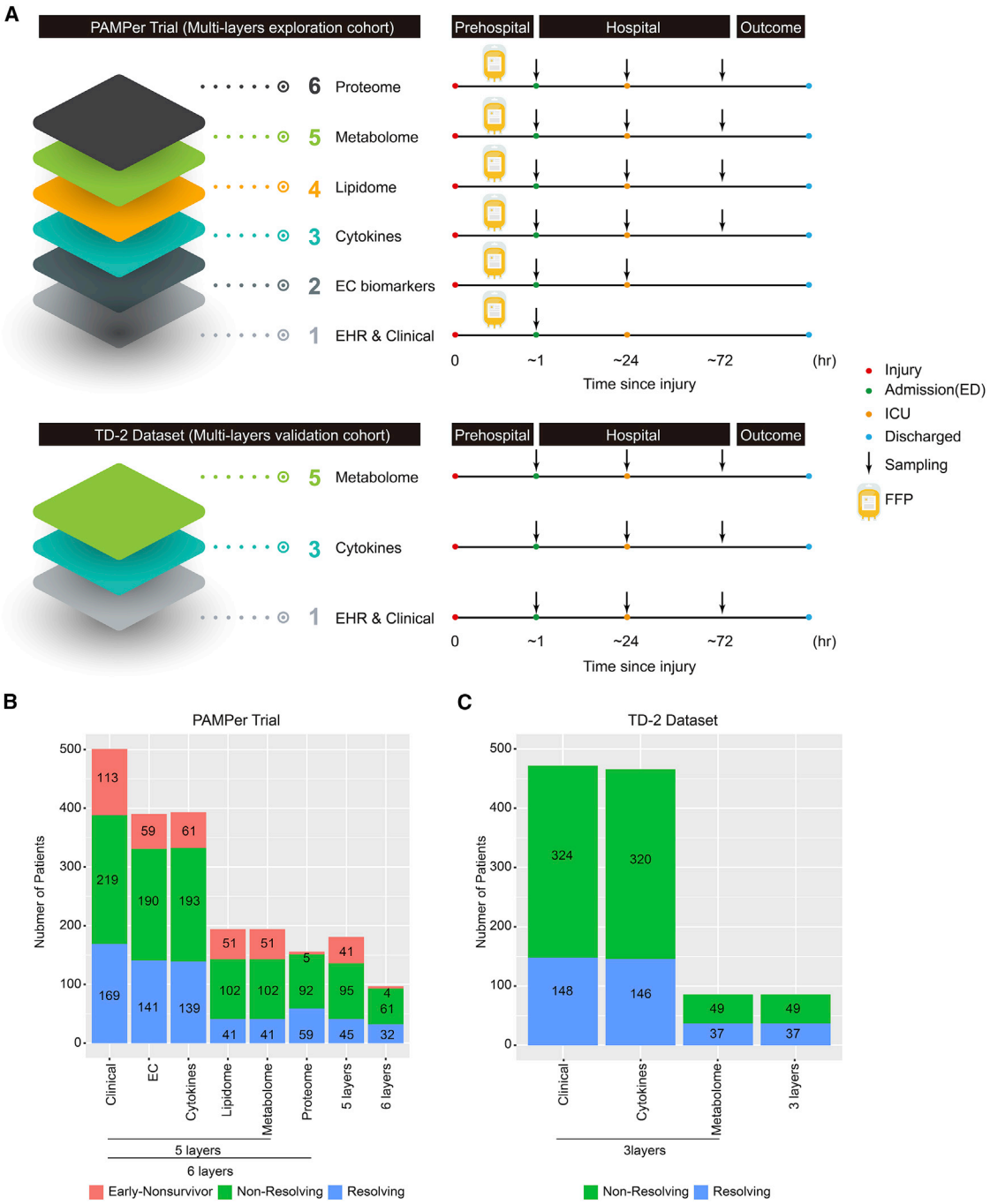

Figure 1. Overview of study design and cohort details

(A) Scheme illustration of data layers showing longitudinal sampling of trauma patients in the exploration cohort (PAMPer, top panel) and validation cohort (TD2: bottom panel). EC, endothelial cell; her, electronic health record.

(B and C) Distribution of patients for the exploration cohort (B) and validation cohort (C) by data layer, number of patients, and outcome.

in early nonsurvivors was especially obvious. Remarkably, the levels of all metabolites represented in modules 3 and 4 returned to the low baseline levels observed in HCs by 24 and 72 h after admission. Modules 6 and 7 were higher in HCs. Levels of these metabolites were lower in trauma patients at time 0 h and later. The large number of metabolites in module 5 had no distinguishable patterns related to outcome or time. The relative changes based on average *Z* scores for the metabolites in all 7 modules are shown for both PAMPer and TD2 datasets in Figures 2E and 2F, confirming the patterns observed in the heatmaps.

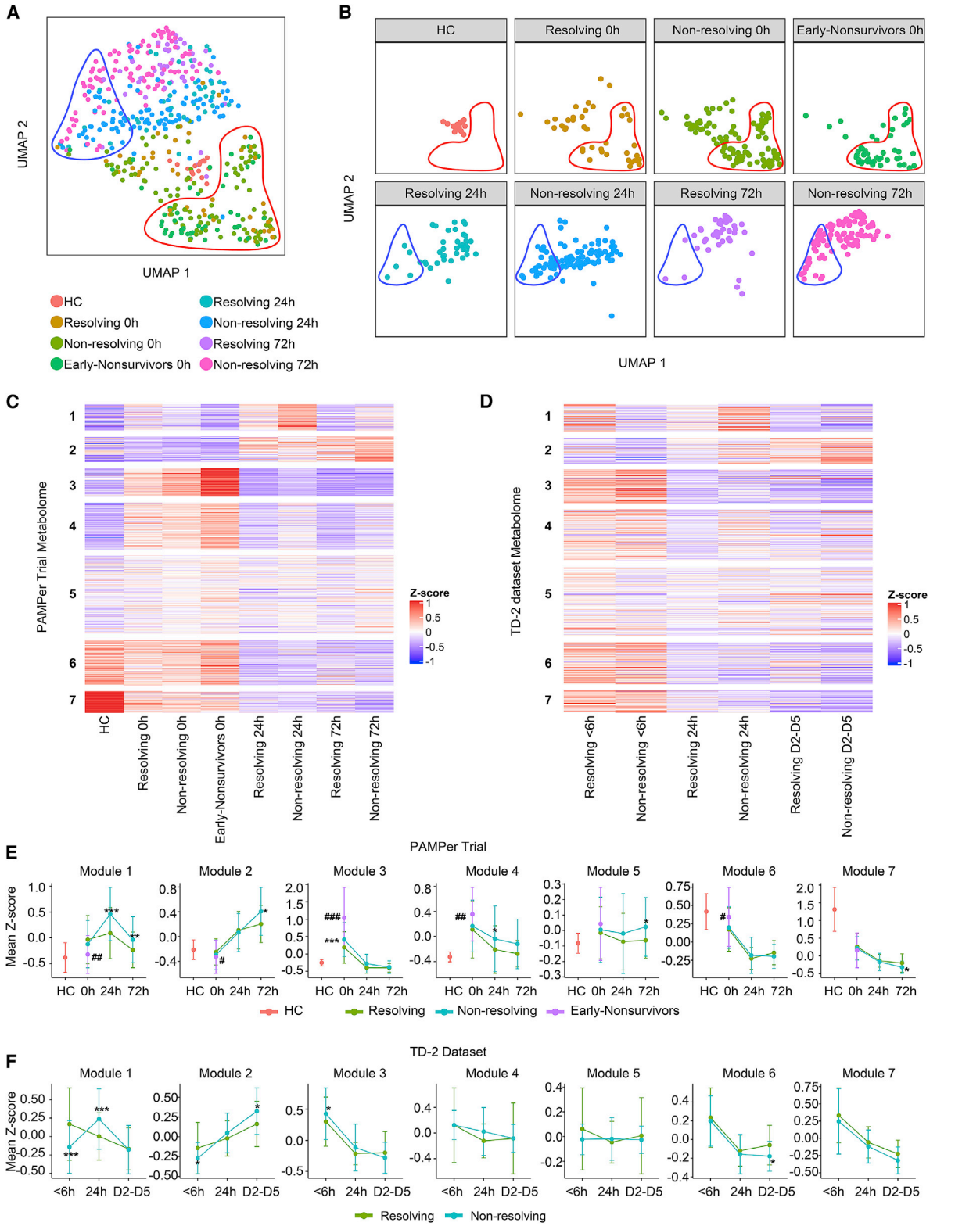

Figure 2. Global temporal patterns within the circulating metabolome based on patient outcomes

(A and B) Uniform manifold approximation and projection (UMAP) plots show the distribution of healthy controls (HCs; n = 17) and patients with trauma (n = 194). All subjects (A) and separated by time and outcome (B). Numbers of subjects in each group: 17 (HCs), 41 (resolving 0 h), 102 (non-resolving 0 h), 51 (early

(legend continued on next page)

Similar patterns across all seven modules were observed when patients were segregated by injury severity, with greater injury severity corresponding to worse outcomes (Figures S3D and S3E).

The top metabolic and biosynthetic pathways represented in each module are shown in Figure 3A. We also provide a list of all the metabolites in the seven modules (Table S4). Modules 1 and 2 were highly represented by lipids (66.7 and 34.8%, respectively), while modules 3 and 4 included molecules from all major subclasses (Figure S3A). Module 5 was mostly xenobiotics (49%) that mainly consisted of drugs unrelated to trauma management (Figures S5A and S5D). Many of the metabolites in modules 6 and 7 were plant- and xanthine-related xenobiotics, suggesting that the lower levels in trauma patients represents the fasting state that is part of routine clinical management (Figures S5A and S5D). To demonstrate the patterns of representative metabolites from modules 3 and 4, energy metabolites comprising the tricarboxylic acid (TCA) cycle and glycolysis/gluconeogenesis-related carbohydrates were projected onto heatmaps and line plots (Figures 3B and 3D). Most of these metabolites were higher at 0 h, with the highest levels in early nonsurvivors. The levels of five metabolites (malate, succinate, citrate, fumarate, and *cis*-aconitate) from the TCA cycle were further validated in a quantitative assay (Figures S5B and S5C). In addition, multiple metabolic intermediates from lipid and amino acid metabolism were markedly elevated in the non-resolving patients and early nonsurvivors at 0 h compared with HCs (Figure 3A; Table S4). There were also a small number of xenobiotics enriched in modules 1–4, and many of these were related to anesthetics or antibiotics (Figures S5E–S5F).

We next assessed the relative levels of metabolites across specific pathways represented in modules 1 and 2. Heatmaps for the polyunsaturated fatty acids (PUFAs), corticosteroids, and acyl cholines demonstrated an increase in only a subset of metabolites from these pathways, suggesting an active release and re-utilization of certain lipids, especially at 24 h (Figures 3C and 3D). The higher levels of stress hormones, cortisol and cortisone, at 24 and 72 h may reflect an ongoing stress response in patients slow to resolve. Numerous choline-bound fatty acids were higher in resolving patients, suggesting an active process involving lipid release in the recovery phase. Interestingly, we also identified two carbohydrates associated with protein glycosylation, glucuronate and mannose, in module 1 and module 2 at 24 and 72 h. These were higher in the non-resolving patients, which may reflect a change in the turnover of glycoproteins (Figures 3B and 3D).

Dramatic perturbation of the plasma proteome triggered by severe injury

We next analyzed the dynamic patterns in plasma protein levels (n = 1,305) within a subset of PAMPer patients (n = 151; Table S2). To examine the reliability of the proteomic analysis, we correlated the values for six highly upregulated inflammatory mediators in the plasma between the quantitative Luminex platform (cytokine layer) and the Somascan proteomic analysis (proteome layer). There was high correlation for all six cytokines/chemokines (interleukin-6 [IL-6], IL-8, IL-10, MCP-1, MIG, and IP10; Figure S6A).

An assessment of the global changes in plasma proteomics revealed that major differences were time, outcome (Figure 4A), and injury severity associated (Figures S6B and S6C). There was an obvious increase of most proteins (n = 880) in the circulation early that was notably greater in patients that were more severely injured or that had a slower clinical recovery (Figure 4A; Figures S6B and S6C; Table S6). However, a smaller subset of distinct proteins (n = 95) was higher at 72 h after injury. Pathway enrichment analysis for the upregulated proteins at 0 h indicated that elevated proteins are constituents of many intracellular pathways such as apoptosis, necroptosis, IL signaling, interferon (IFN) signaling, and kinase signaling (Figure 4B).

Next, we assessed changes in circulating proteins by class as a function of time and outcome. A subset of proteins within each class were annotated by their families (Figures 4C–4J; Table S8) and revealed a near indiscriminate release of cellular proteins early. Proteins that fit this pattern associated with cell stress and death (e.g., S100/heat shock protein [HSP]/Bcl2/cathepsin/caspase/HMGB family; Figure 4C), intracellular constituents (e.g., membrane: annexin/CD surface proteins; cytoplasm: EIF family; ribosome: RPS/L family; mitochondrial: CYP enzyme family; nuclei: histones; Figure 4D), inflammatory mediators (e.g., IL/CCL/CXCL/tumor necrosis factor [TNF]/INF families; Figure 4E), receptors for inflammatory mediators (e.g., IL/TNF/IFN receptor families; Figure 4F), intracellular enzymes (kinases) (e.g., mitogen-activated protein kinase [MAPK]/AKT/GSK/PTK families; Figure 4G), and endothelial cell injury- and adhesion-related molecules (e.g., VEGF/PDGF/ICAM/VCAM/CDH families; Figure 4H). Levels of most of these proteins dropped by 24 h, and a separate and smaller subset of proteins became elevated at 72 h, often higher in patients with slow recovery. In striking contrast, most of the proteins from the apolipoprotein, coagulation, fibrinolysis, and complement pathways showed outcome-specific patterns across time (Figures 4I and 4J). Levels of many of these proteins were low at 0 h and became markedly elevated by 72 h, and to a

nonsurvivors 0 h), 41 (resolving 24 h), 101 (non-resolving 24 h), 41 (resolving 72 h), and 101 (non-resolving 72 h). Area encircled by red line shows time 0 h distribution from non-resolving patients and early nonsurvivors, and area encircled by blue line shows 24 and 72 h distribution of non-resolving patients.

(C) Heatmap shows relative levels of individual metabolites for HCs and trauma patients in the exploration cohort, grouping by outcome and sampling time points. Numbers of subjects in each group are same as in (A). Rows are clustered by K-means clustering (k = 7).

(D) Heatmap shows the validation cohort (TD2) representing the metabolites in common with the exploration (PAMPer) cohort from (C). Numbers of subjects in each group: 61 (resolving 0 h), 48 (non-resolving 0 h), 60 (resolving 24 h), 48 (non-resolving 24 h), 52 (resolving 72 h), and 37 (non-resolving 72 h).

(E and F) Comparison of signature scores for the 7 metabolite modules (from A) in the exploration cohort (E) and validation cohort (F). Numbers of subjects in each group from PAMPer dataset are same as in (A). Numbers of subjects in each group from TD2 dataset are same as in (D). Patients are grouped by outcome and sampling time points. The y axis is labeled as *Z* score. Data are shown as mean ± SEM. Hashes indicate statistical significance between patients of early nonsurvivors and resolving pattern based on Kruskal-Wallis (K-W) test among 3 groups at 0 h with post hoc analysis of Dunn test. The p value was adjusted by Benjamini-Hochberg method: #, < 0.05; ##, < 0.01; ###, < 0.001. Asterisks indicate statistical significance based on 2-way AVOVA of time-series analysis of resolving and non-resolving groups. Pairwise comparisons were conducted by estimated marginal means test. The p value was adjusted by Benjamini-Hochberg method: *, < 0.05; **, < 0.01; ***, < 0.001.

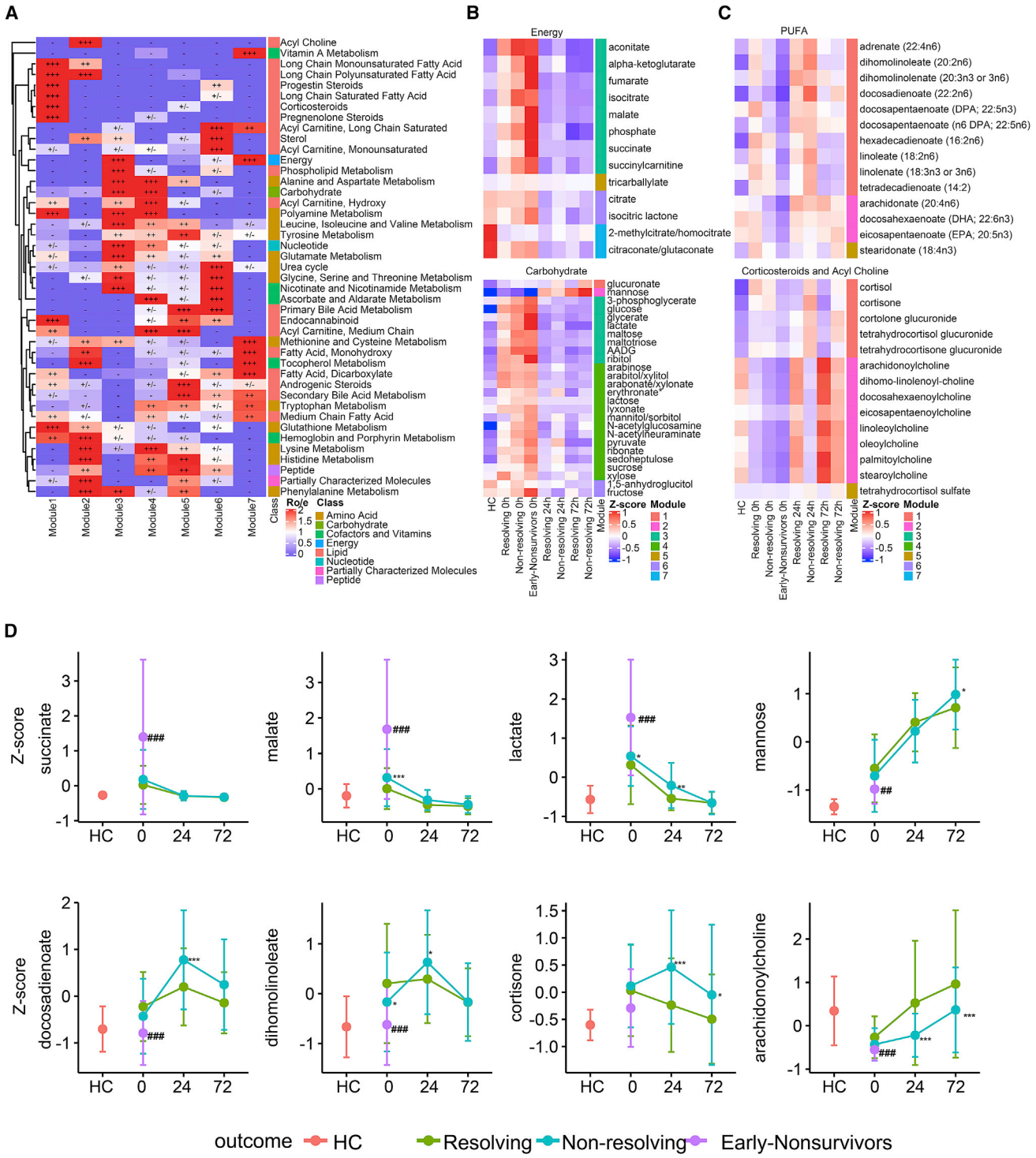

Figure 3. Metabolite patterns by module and over time after severe injury

(A) Heatmap shows the enrichment metabolites from the indicated pathways (excluding xenobiotics) in the 7 metabolite modules. +++, Ro/e > 2; ++, 1.2 < Ro/e < 2; +\–, 0.8 < Ro/e < 1.2; –, 0.5 < Ro/e < 0.8; —, Ro/e < 0.5.

(B) Heatmap shows temporal pattern of selected metabolites from energy and carbohydrate pathways. Patients are grouped by time point and outcome. Numbers of subjects in each group: 17 (HCs), 41 (resolving 0 h), 102 (non-resolving 0 h), 51 (early nonsurvivors 0 h), 41 (resolving 24 h), 101 (non-resolving 24 h), 41 (resolving 72 h), and 101 (non-resolving 72 h).

(legend continued on next page)

greater degree in patients that resolved early (e.g., APOE/APOD/C2/C5/F5/F9). It is notable that proteins associated with fibrinolysis (e.g., plasmin/tissue plasminogen activator [tPA]/urokinase plasminogen activator [uPA]; Figure 4J) were higher in the slower-resolving patients at time 0 h and these dropped by 72 h. Taken together, our global analysis of protein levels reveals a broad early release of cellular constituents especially prominent in patients that recover slowly. The relative paucity of apolipoproteins, coagulation factors (CFs), and complement factors early after injury may represent consumption due to pathway activation.

Distinct severity-associated systemic storm and coagulopathy-associated massive consumption patterns resolved by integrated multi-layer analysis

To further identify the dominant features in the hyper-acute phase of trauma, we conducted an integrated correlation analysis for patients (n = 88) with all six data layers at 0 h in the PAMPer dataset. All variables from the six data layers at 0 h were correlated with injury severity (ISS), lactic acidosis (lactate levels), or coagulation abnormalities (inverse correlation with INR). A total of 1,061 markers were correlated with ISS or lactate, and 892 markers were inversely correlated with INR (false discovery rate [FDR] < 0.05). Many of the markers from the metabolome layer showed a similar pattern in the TD2 dataset. The top 200 correlated variables each for ISS, lactate, and INR were used to build a correlation heatmap (Figure 5A). Two clear patterns emerged, one large set of variables positively associated with ISS and lactate and another set of variables inversely correlated with INR. Based on our biologic interpretation, we labeled the former pattern "systemic storm" to reflect the extensive simultaneous release of cellular constituents into the circulation in association with injury severity. Because the second pattern reflected factors lost from the circulation with increasing INR, we named this pattern "massive consumption." The systemic storm pattern included subset 1 cytokines (IL-6, IL-8, IL-10, MCP-1/CCL2, MIG/CXCL9, and IP-10/CXCL10), EC injury biomarkers (syndecan-1, sVEGFR, and thrombomodulin [TM]), tissue-specific injury proteins (brain: glial fibrillary acid protein [GFAP]; heart: troponin [TnT]; muscle: ceatine kinase B [CKB]; liver: cytochrome P450 oxidoreductase [CYPOR]; kidney: cystatin family), cell compartment components (nucleus: histones, TATA-box-binding protein [TBP], histone-complexed DNA [HC-DNA]), cell stress and death proteins (HSP, S100, and Bcl2 families), IFNs (IFN alpha, beta, gamma, and lambda), energy substrates (glucose, lactate, pyruvate, and ribitol), and metabolic intermediates (glycerol-3-phosphate). The massive consumption pattern consisted of lipids (triacylglycerol [TAG], diacylglycerol [DAG], and cholesterols), lipid transportation proteins (APOA), complement factors, CFs, serpins, and Kalikrein-Kallistatin (K-K) system enzymes. We separately analyzed the correlation of three representative systemic storm markers (histone 1-2 [H1-2], HSPB1, and IFNL1) with ISS (Figure 5B). A sharp upward slope for all three was observed to correlate with ISS between 0 and 25. Above 25, the ISS score typically accepted as the threshold between moderate and severe injury, the correlation curves flattened. Plasminogen, uridine, and C3b from the massive consumption cluster markedly dropped, with INR values between 0.9 and 1.5, followed by a flattening in the curves at INR above 1.5. Thus, there are two dominant and dramatic patterns that emerge in the circulation within h of injury: one highly sensitive to the degree of injury and resulting in increases in hundreds of circulating metabolites and proteins, and the other reflecting a loss of plasma constituents that correlates with the degree of coagulopathy.

To explore the potential source of released circulating factors in the systemic storm pattern, we selected 30 representative markers and ranked these based on their correlation with plasma HC-DNA, a marker of necrotic cell death,[26] at 0 h (Figure 5C). Histones (H1-2 and H2AW), HMGB1, the transcription factors EIF4A3 and TBP, and the chemokine CXCL5 were highly correlated with HC-DNA ($r > 0.6$), suggesting that these factors might be released passively during lytic cell death. The IFNs (IFNL1, IFNA2, IFNB, and INFG), proinflammatory cytokines/ chemokines (IL-10, IL-6, IL-8, MCP-1/CCL2, and IP10/CXCL10) were moderately associated with HC-DNA ($0.3 < r < 0.6$), consistent with a mixed passive-plus-active release pattern. The energy metabolites and carbohydrates (lactate, malate, glucose, and succinate) were weakly correlated with HC-DNA, indicating that the source of their release may not be lytic cell death. We next conducted a network-based correlation analysis for both the proteins and metabolites from the injury severity-related systemic storm pattern. The top 20 factors that correlated with inflammation (based on IL-6), injury severity (ISS), or lytic cell-death (HC-DNA) showed excellent inter-category correlation (Figure 5D). However, the top 20 metabolites from the energy (based on succinate) or carbohydrate (based on lactate) categories were highly correlated with each other, but weakly correlated with inflammation, ISS, or cell-death-associated factors (Figure 5D). Taken together, these findings indicate that the metabolites and proteins released in systemic storm pattern may reflect two distinct biological processes triggered by severe injury.

Resolution and non-resolution signatures at 72 h aligned with clinical recovery

We next conducted a similar correlation analysis using 72 h data from five layers (clinical, cytokine, lipidome, metabolome, and proteome; n = 51) to explore the patterns related to recovery. Here, we correlated all factors from the five layers with length of stay in intensive care unit (ICU LOS), a parameter that correlates with patient recovery.[27] For the patients that died beyond

(C) Heatmap shows temporal pattern of selected metabolites from PUFA and corticosteroid families. Patients are grouped by time point and outcome. Numbers of subjects in each group is same as in (B)

(D) Comparison of 8 selected representative metabolites from trauma response modules 1–4. Patients are represented by outcome and time point and are compared with HCs. Numbers of subjects in each group are same as in (B). Data are shown as mean ± SEM. Hashes indicate statistical significance between patients of early nonsurvivors and resolving pattern based on K-W test among 3 groups at 0 h with post hoc analysis of Dunn test. The p value was adjusted by Benjamini-Hochberg method: #, < 0.05; ##, < 0.01; ###, < 0.001. Asterisks indicates statistical significance based on 2-way AVOVA test of time-series analysis of resolving and non-resolving groups. Pairwise comparisons were conducted by estimated marginal means test. The p value was adjusted by Benjamini-Hochberg method: *, < 0.05; **, < 0.01; ***, < 0.001.

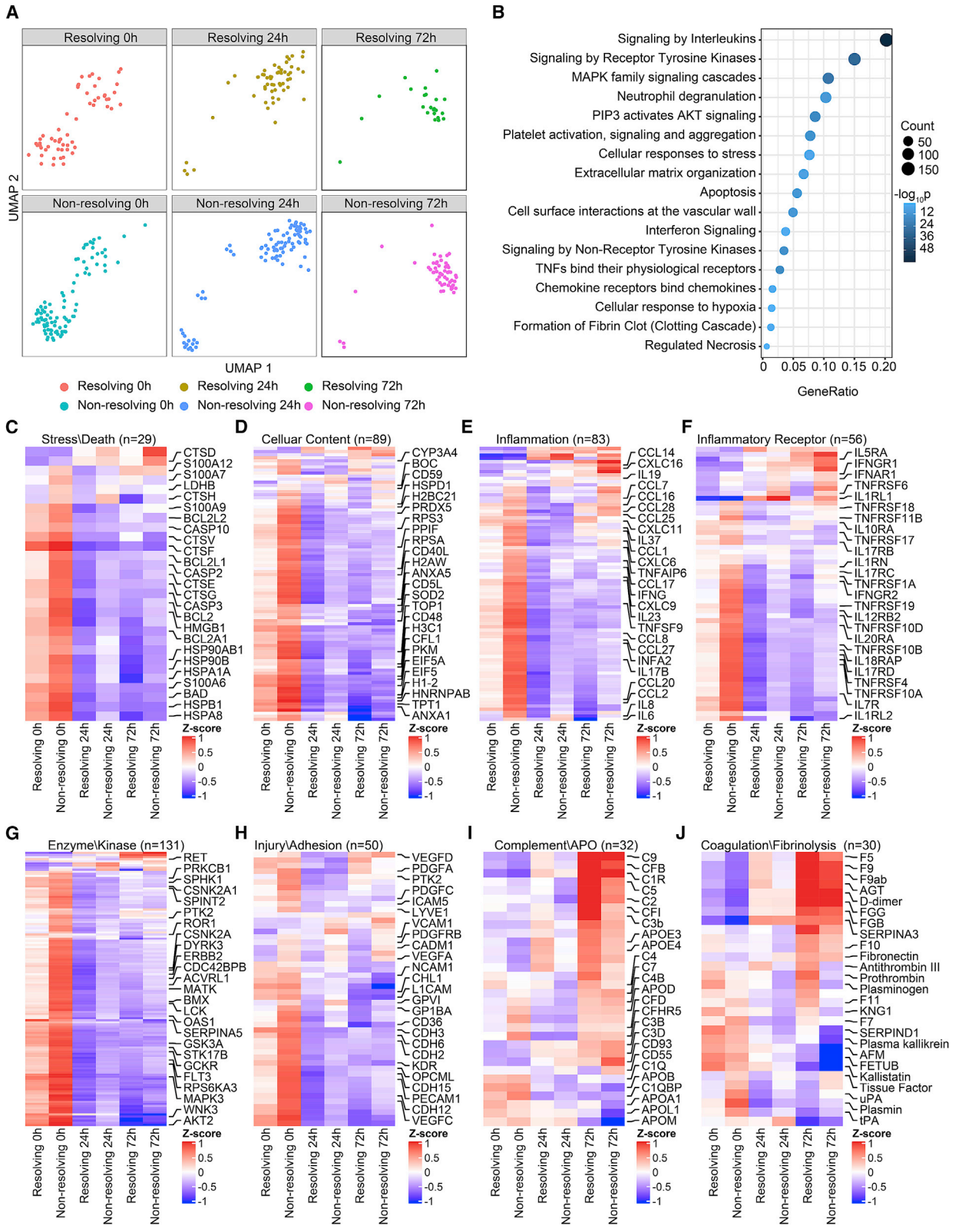

(legend on next page)

72 h (n = 9), the ICU LOS was set at 30 days, the trial observation endpoint. All variables positively (n = 176) or negatively (n = 52) correlated with ICU LOS (FDR < 0.05) were selected to build a correlation heatmap (Figure S7A). Variables positively correlated with ICU LOS were defined as non-resolution signatures, and those negatively correlated with ICU LOS were defined as resolution signatures. Interestingly, the non-resolution signatures included many factors seen in the systemic storm pattern at 0 h (e.g., GFAP, IL-6, and IL-8). However, this large group also consisted of many unique metabolites, lipids, and protein families that were highest at 72 h (i.e., acute-phase proteins: soluble ST2; chemokines: CXCL13 and CXL19; growth factors: SCF-a [stem cell growth factor alpha] and SDF-1 [stromal cell-derived factor-1]; hormones: resistin and glucagon; bacteria-derived metabolites: imidazole lactate; M2 macrophage associated: CD206 and MMP12; and lipids from the lipid reprogramming signature (LRS) defined in our previous analysis of the lipidomics of critical illness.[23] The resolution signature included factors also identified in the massive consumption pattern from 0 h (e.g., complement components, CFs, and K-K system proteins). It is notable that there were differences in the specific proteins from these families between the 0 and 72 h time points. We also observed many lipids (lyso-phospholipids, cholesterol esters, and sphingolipids) in the resolution signature cluster. We have previously shown that elevated sphingolipids (e.g., sphingosine-1-P) associate with better outcomes after trauma.[24] Representative markers for both signatures were found to have a linear correlation with ICU LOS (Figure S7B). Similar to the analysis at 0 h, correlation of top biomarkers with histone (H1-2), a protein known to be released during lytic cell death,[26] implicated both passive and active processes (Figure S7C). However, in contrast to the 0 h pattern, the release of factors across categories of molecules appears to be more interconnected, indicating there may be well-coordinated processes during the later adaptive response post injury (Figure S7D).

Early systemic storm and massive consumption patterns associate with mortality and delayed resolution

To identify the patterns within the data layers that most closely associated with outcomes, we constructed signature scores that captured the major findings from each data layer (Table S7). The proteome layer was excluded to optimize patient numbers and to avoid redundant information with the cytokine and EC layers. For mortality, we observed two clear patterns: one associated with the systemic storm (ISS, Glasgow Coma Scale [GCS], severe head injury, subset 1 cytokines, EC biomarkers, modules 3 and 4 metabolites), and the other with massive consumption (INR, coagulopathy, transfusions in the first 24 h, and lipid concentration) (Figure 6A). The data features that were associated with either systemic storm or massive consumption had a strong internal correlation but exhibited weak inter-pattern correlation (Figures 6A and 6B). Interestingly, both patterns were positively correlated with 3- and 30-day mortality. While there was a strong positive correlation among subset 2 (lymphocyte-related) and subset 3 (reparative) cytokines, these mediator subsets were negatively correlated with EC biomarkers, metabolite release, and clinical coagulopathy.

We next explored the importance of each variable within the four layers (cytokines, EC, metabolome, and lipidome) to predict early death using weighted rankings based on five statistical/machine learning methods (receiver operating characteristic [ROC] curve, logistical regression with lasso regularization, logistical regression with elastic-net regularization, SIMPLS algorithm from partial least-squares regression, and random forest). MIG, syndecan-1, TAG50:4-FA20:4, and *N*-acetylaspartate (NAA) were the most important variables from the cytokine, EC, lipidome, and metabolome layers, respectively (Figure 6C). A logistical regression model with elastic-net regularization was applied for prediction of early mortality. Of the five data layers, the metabolome layer contained the information with the highest area under the curve (AUC) for early mortality (AUC value = 0.798). When information from all five layers was included in the model, the AUC value reached 0.867 for early mortality (Figure 6D). The combination of fewest individual components that had the highest AUC incorporated GCS, INR, and NAA (module 3 metabolite) (AUC value = 0.848); adding MIG/CXCL9, syndecan-1, and TAG50:4-FA20:4 increased the AUC value to 0.858 (Figure 6E). Taken together, this predictive modeling shows that sensitive indicators of brain injury/response (GCS and NAA) and coagulation abnormalities (INR) have the closest association with early death.

To explore the relationship between the systemic storm features and non-resolution-related factors across five data layers (excluding the proteome layer), we conducted a correlation analysis using data from all three time points in patients surviving to 72 h (Figures S8A and S8B). There was a strong correlation among the major data components across time (modules 1, 3, and 4 metabolites at 24 and 72 h; modules 1, 3, and 4 metabolites at 0 h; EC biomarkers at 0 and 24 h; and subset 1 cytokines at all 3 time points). There was also a "lead effect" in that the patients exhibiting a higher magnitude of perturbation at 0 h were likely to have a relative higher magnitude response at 24 or 72 h. The overlapping factors within the early (0 h) and late adverse patterns (24 or 72 h) also positively correlated with late outcomes (ICU LOS and nosocomial infection [NI]; Figures S8A and S8B).

We next explored the importance of factors for predicting non-resolution based on the 0 h data only (Figure S8C). The lipidome

Figure 4. Global temporal pattern of circulating proteome associated with outcomes

(A) UMAP plot show the distribution of proteome in patients with trauma, split by outcome and sampling time points. This map is a 2D projection of the whole proteome, and each dot represents one sample. Here, the distance between each dot reflects the difference of the proteome between two samples. Numbers of subjects in each group: 59 (resolving 0 h), 92 (non-resolving 0 h), 56 (resolving 24 h), 90 (non-resolving 24 h), 23 (resolving 72 h), and 53 (non-resolving 72 h).

(B) Main Gene Ontology (GO) pathways represented by the top 880 proteins identified at time 0 h, resolving versus non-resolving patients.

(C–J) Heatmap shows temporal and outcome-based patterns of circulating proteins by protein families. Representative proteins are labeled on the y axis. Numbers of subjects in each group are same as in (A). Cell stress and death (C), intracellular constituents (D), inflammatory mediators (E), receptors for immune mediators (F), enzymes (kinases) (G), cell adhesion (H), complement factors and apolipoproteins (I), and coagulation factors and fibrinolysis regulators (J). Entrez gene symbols were applied for available proteins (Table S5).

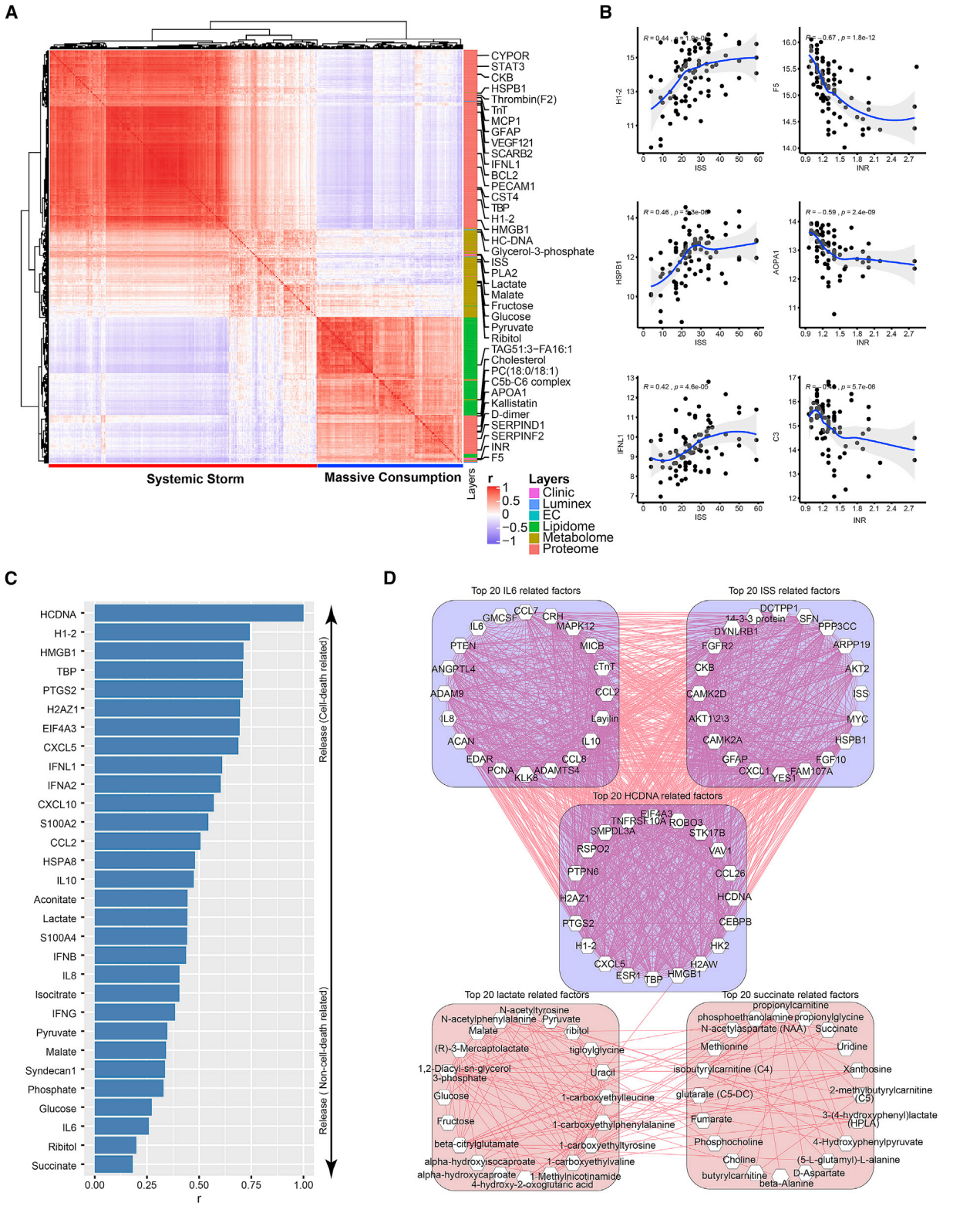

(legend on next page)

layer was excluded since it did not contain data that contributed to outcome prediction. Interestingly, MCP-1, syndecan-1, and NAA were the most important variables for predicting slow resolution. As shown above, the latter two were also the most predictive variables for early death. The clinical, cytokine, and EC injury data layers had higher AUC for non-resolution than the metabolome layer (Figure S8D). Using a combination of single variables from the clinical (GCS), cytokine (MCP-1), EC injury (syndecan-1), and metabolomics (NAA) data layers reached an AUC value of 0.851 (Figure S8E) and matched the AUC value obtained using all variables within the data layers (AUC = 0.849; Figure S8D). Taken together, these findings indicate that features of the multi-omic analysis can be used to identify individual variables that most closely associate with distinct adverse outcomes and that predictive variables may differ by outcome.

Multi-layer characterization-derived patient endotypes associate with distinct clinical trajectory

To test whether the multi-layer data obtained at time 0 h would be useful to identify clinical trajectory-related endotypes, we subjected the factors positively associated with the systemic storm (Figure 5A) along with subsets 2 and 3 cytokines to consensus K-means clustering (Figure 7A). This yielded two major patient clusters designated as endotype 1 (E1; n = 91) and endotype 2 (E2; n = 82) that were independent of brain injury (Figure 7A). E1 positively associated with subsets 2 and 3 cytokines and negatively with EC injury biomarkers, subset 1 cytokines, and modules 3 and 4 metabolites and exhibited significantly lower 30-day mortality (Figure 7B). On the contrary, E2 patients were positively associated with higher levels of EC injury biomarkers, subset 1 cytokines, and modules 3 and 4 metabolites and much higher mortality than E1 patients ($p = 0.00048$). In fact, endotype aligned better with 30-day mortality than grouping patients based on ISS severity (Figure 7B; Figure S9A). Multi-variable Cox regression analysis further suggested that endotype, coagulopathy, and brain injury, but not ISS, were independent risk factors for mortality (Figure S9B). Prehospital TP administration was the only independent factor positively associated with survival (Figure S9B).

Prehospital TP administration only benefits the E2-TBI subgroup

We previously reported that prehospital TP administration provided a survival benefit to patients with traumatic brain injury (TBI).[28] We next sought additional insight on the characteristics of the patients that benefitted from TP administration. Four subgroups based on endotype and the presence or absence of TBI were identified. As shown in Table S3, E1-NBI (no brain injury) comprised lower-injury-severity patients without brain injury; E1-TBI patients were more likely to have isolated TBI or mild non-brain injury; E2-NBI patients had severe injury, but without TBI; and the E2-TBI group included TBI patients with moderate-to-severe non-brain injury. In dramatic effect, prehospital TP only improved survival in the E2-TBI group, with a 69% risk reduction (44.6% net reduction in 30-day mortality; log rank $p = 0.0015$; hazard ratio [HR] = 0.31; 95% confidence interval [CI]: 0.12–0.81; Figures 7C and 7D).

We next explored the potential mechanisms of the selective protective effect of TP on TBI patients. As expected, prehospital TP was associated with lower admission INR in both NBI and TBI than in patients that received standard of care (Figure S9C). Interestingly, we found that TP seemed to have trend ($p = 0.14$) toward mitigating the magnitude of clinical coagulopathy in TBI patients (Figure S9E). We next assessed the impact of prehospital TP on EC/cytokine, lipidomic, metabolomic, and proteomic patterns as well as levels of brain-specific injury biomarkers in the circulation (GFAP and ubiquitin carboxy-terminal hydrolase L1 [UCHL1]). Patient groups are shown based on treatment with or without TBI at 0 and 24 h (Figure 7F; Figure S9D). Prehospital TP had limited effects on cytokines or EC injury markers in both TBI and NBI patients. In addition, no obvious alterations in GFAP and UCHL1 levels were observed in TBI patients between the two treatment arms in either E1 or E2 patients (Figures S9F and S9G). While no consistent change in global patterns of metabolites emerged with TP, there was a distinct change in the patterns of lipids that was unique (higher levels of lipids) for TBI patients that received prehospital TP at both 0 and 24 h (Figure S9D; Table S9). The presence of TBI associated with a marked increase in the levels of many proteins that were elevated only at the 0 h time point (a representative subset shown in Figure S9D). Most of these proteins were associated with cell death/stress, and this was not impacted by prehospital TP. However, there was also a selective increase in 41 proteins observed only in the TBI patients that received TP (Figure 7E). Of note, this plasma effect was not observed in NBI patients receiving TP, and the differences were observed at both 0 and 24 h, demonstrating that the TP effect on levels of these proteins persisted beyond admission. Proteins in this group included CFs and complement factors as well as several CCL chemokines and members of the serpin family, among others. Thus, the administration of TP to E2 patients with TBI resulted in an increase in circulating levels of subsets of lipids and proteins that persisted to 24 h.

We provide a brief summary of our major findings on the potential mechanisms of the prehospital TP effect in Figure 7F.

Figure 5. Cross-platform plasma multi-omics data integration reveals pattern of systemic storm and massive consumption in the hyperacute phase

(A) Correlation heatmap incorporating the top features in 88 patients that correlate ISS or lactate of inversely correlate with INR (200 features each for ISS, lactate, or INR) at time 0 h. The variables were derived from all six data layers, and the correlations were based on Spearman correlation coefficients. Two major patterns emerged: one positively associated with ISS (systemic storm) and the other inversely correlated with INR (massive consumption).

(B) Three systemic storm variables were correlated with ISS, and three massive consumption variables were correlated with INR.

(C) Ranking of 30 variables in systemic storm pattern based on the correlation with the necrosis marker HC-DNA; r values derived as Spearman correlation coefficients.

(D) Five correlation nodes (20 variable each), shown as circle plots, were constructed based on correlation to a lead feature for network as follows: IL-6, ISS, HC-DNA, lactate, and succinate. Lines between two nodes indicate strong correlation ($r > 0.6$).

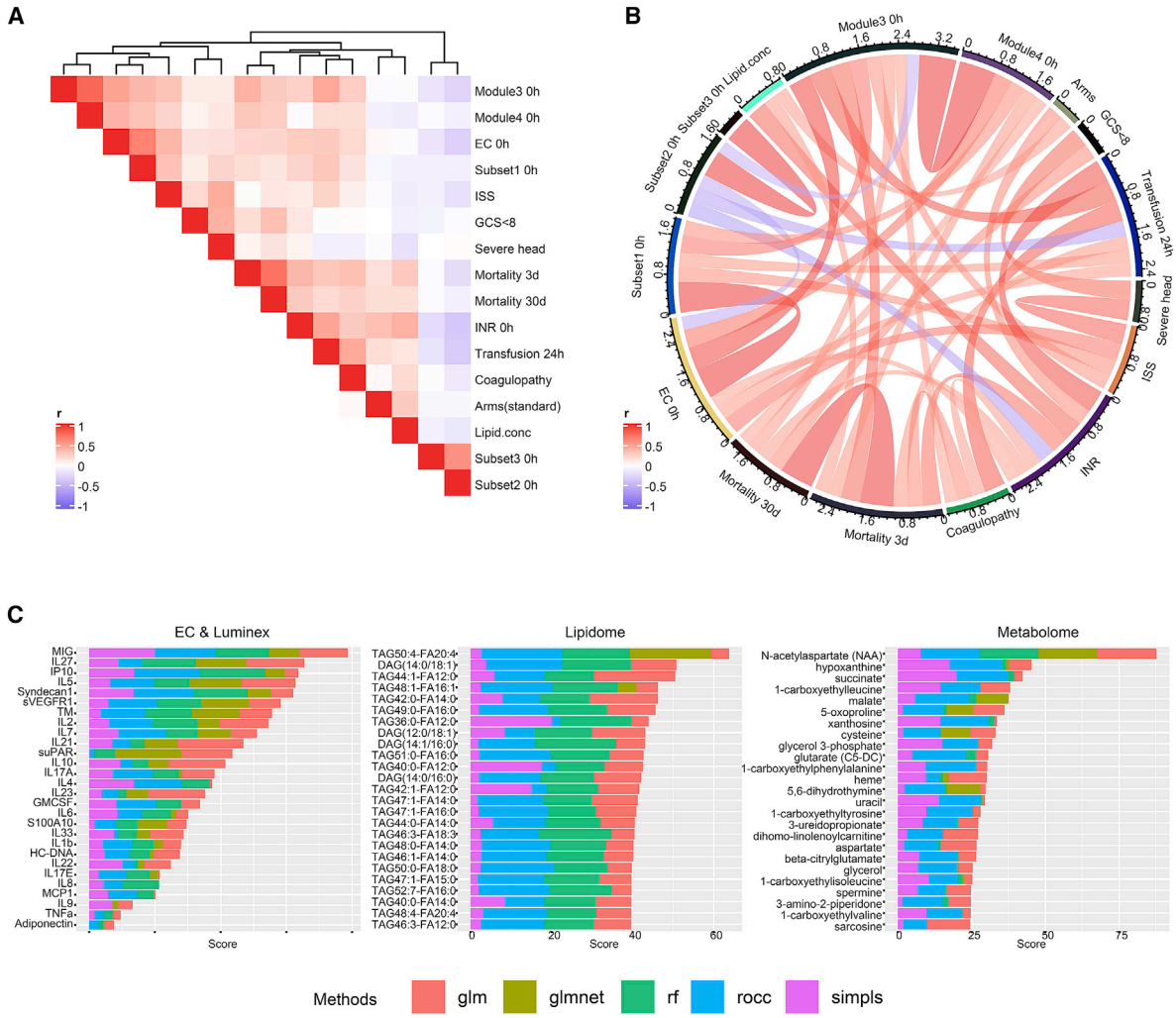

(legend on next page)

We speculate that E2-TBI patients may have a pattern of coagulopathy that is sensitive to correction by early TP administration. This effect is not observed in E2-NBI patients, despite the early correction of the INR. The differential response of E2-TBI patients observed through this multi-omic analysis of plasma includes a preservation of plasma lipids and CFs and complement factors. Whether TP has a direct benefit to brain-injury-specific responses requires more evidence.

Early stratification of patients to identify those most likely to benefit from early TP

Because it is not routine to carry TP in the field, due to the expense and challenging logistics, there would be value to the development of point-of-care diagnostics to identify patients that are highly likely to benefit from early administration of TP. Therefore, we sought to build a classifier for early stratification using 2 brain-injury-specific biomarkers, 21 cytokines, and 7 EC injury-related biomarkers measured at 0 h (n = 173 trauma patients). Median value was used to impute missing data of GFAP and UCHL1 for TBI (n of missing data = 9) or NBI (n of missing data = 72) patients, respectively. We adopted a two-step machine learning approach based on feature selection followed by classification using the down-selected features. We used the standard-of-care patient subset as a training dataset and the patients in TP arm as the test set. The top selected features by all models (accuracy > 0.8) in each subgroup were UCHL1 (brain-specific biomarker), sydencan-1 (EC biomarker), IL-17A (subsets 2 and 3 cytokine), and IP10/CXCL10 (subset 1 cytokine) (Figure S10A).

We next built three models for predicting patients likely to benefit from TP (E2-TBI subgroup) by logistic regression that included the following: (1) systemic biomarkers only: syndecan-1, IP10, and IL-17A; (2) brain-specific marker only: UCHL1; and (3) a combination of (1) and (2): UCHL1, syndecan-1, IP10, and IL-17A. We found that the brain-specific biomarker UCHL1 alone had an excellent predictive value in both the training and test datasets (AUC value of training set: 0.915; AUC of test set: 0.940; Figures S10B and S10C). The combination of 3 systemic biomarkers (syndecan-1, IP10, and IL-17A) had a lower AUC value than UCHL1 (AUC of training set: 0.829; AUC of test set: 0.775; Figures S10B and S10C). The combination of UCHL1 with the three systemic biomarkers slightly improved the prediction value compared with UCHL1 alone (AUC of training set: 0.951; AUC of test set: 0.958; Figures S10B and S10C). These data suggest that early measurement of the brain-specific biomarker UCHL1 identifies patients with brain injury and also accurately identifies patients that could benefit from early TP administration.

DISCUSSION

In this study, we present a comprehensive characterization of the global features of the human response to severe injury by plasma multi-omic analysis. This permitted an exploration of the dynamic patterns in circulating biomolecules that associate with clinical trajectories after severe injury. We identified two early molecular patterns—systemic storm and massive consumption—associated with early mortality and two late patterns (non-resolution and resolution signatures) associated with rate of recovery. The systemic storm pattern reveals the molecular breadth and level of the systemic release of cellular constituents that immediately follows severe injury, a pattern that associates with injury severity and outcomes, yet rapidly resolves by 24 h. Just as biologically interesting is the immediate disappearance from the circulation of lipids[23] and apolipoproteins as well as proteins that make up the proteolytic cascades of the coagulation, complement, and K-K systems revealed in the massive consumption pattern. The identification of outcome and treatment-responsive human injury endotypes yielded both novel biomarkers and biological insights. We show that the presence of TBI in E2 patients markedly changes the human response to early TP and that the brain injury biomarker UCHL1 could be an excellent biomarker for the identification of patients most likely to benefit from early TP. The correlative biomarkers we identified from across the data layers can serve as a guide for precision-based strategies in the early phases of trauma care. The biological insights from our analysis have the potential to identify injury-specific therapeutic targets.

Early increases in circulating cell-death-related damage-associated molecular patterns (DAMPs),[29–33] endothelial injury markers,[34] proinflammatory cytokines/chemokines,[7] and acidosis-related metabolites[35,36] have been previously shown in injured humans. Our current findings indicate that this accumulation of cellular constituents extends well beyond a select few molecules identified to date[37] to 1,061 markers inclusive of nuclear proteins, inflammatory mediators and their receptors, cellular kinases, energy substrates, amino acids, and carbohydrates. We estimate that our observations expand the knowledge on circulating biomolecules that change in human trauma by approximately 10-fold over those previously identified.[38] While some of these biomolecules have been shown to regulate host responses, most have not been studied for their biological activity in systemic responses. Our findings also suggest that the release of many of these molecules is the result of both passive and active processes. However, not all major classes of biomolecules increased in the circulation early after injury. Most notable is the drop in essentially all classes of circulating lipids at time 0 h.[23]

Figure 6. Integrated analysis of mortality-related signatures in the hyper-acute phase

(A) Correlation heatmap that incorporates data subsets from five data layers at time point 0 h (n = 173). Cytokine subsets 1–3, metabolite modules 3 and 4, and lipids represented by total plasma lipid concentration were generalized into individual scores. The r Spearman correlation coefficients were calculated for mortality at 3 or 30 days. Variables are grouped by the data layers.

(B) Correlation circle diagram using the variables from Figure 6A demonstrating the positive and negative correlations between data layer features.

(C) Identification of the variables from the EC+cytokines, lipidome, and metabolome data layers that correlate the most with 30-day mortality. Five statistical/machine learning tools (glm, logistical regression with lasso regularization; glmnet, logistical regression with elastic-net regularization; rf, random forest, simpls, partial least-squares regression; rocc, ROC curve) were applied to the four data layers (EC and cytokines data were combined) and ranked based on the strength of the correlation with mortality.

(D and E) Areas under the curve (AUCs) were calculated for the data layers (D) or highest-ranking features from (C) alone or in combination with GCS and INR from the clinical data layer.

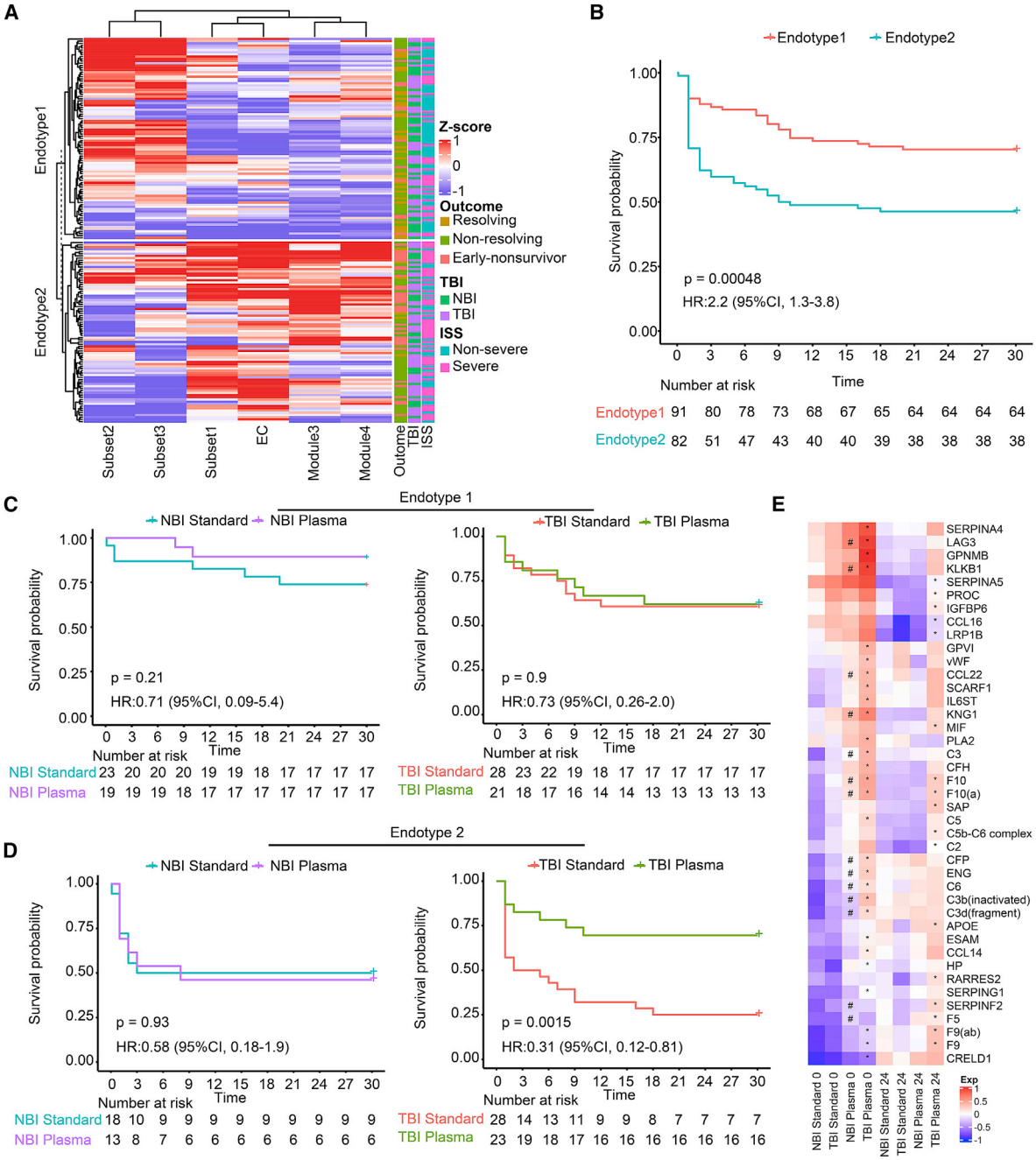

(legend on next page)

Trauma-induced coagulopathy (TIC) is strongly associated with early mortality after trauma.[39,40] Here, we identified a massive consumption pattern that inversely correlated with INR in the hyperacute phase post-trauma. This fits with prior observations and the characterization of "early TIC" as being hypo-coagulable.[41] Many molecules are involved in this process (i.e., CFs, K-K system proteins, complement, and apolipoproteins/complex lipids) through inter-related pathways. However, we found that plasma levels of these molecules only weakly correlated with hyperfibrinolysis-related proteins in the systemic storm pattern, suggesting that these are independent biological processes or weakly connected pathways. Overall, our observations support the concept of well-organized coagulation-complement crosstalk,[42–44] but a weaker association between coagulation-complement activation and inflammation[45] in the early phase post-trauma.

We previously reported that prehospital TP improves the INR in coagulopathic patients, while reducing proinflammatory responses, endotheliopathy, and lipolysis.[21–23] We have also reported that prehospital TP selectively benefits patients with TBI.[28] Here, we significantly advance our understanding of the impact of early TP to show that a specific patient endotype is associated with a favorable response to TP for reduced mortality. Only E2-TBI patients showed a reduction in mortality with TP administration. Furthermore, the TP effect was dramatic in this patient cohort (44.6% net reduction in 30-day mortality). TBI patients that received TP displayed a unique pattern of circulating proteins and lipids compared with non-brain-injury patients that received TP or patients that did not receive TP. The sustained increases in many coagulation- and complement-related proteins in TBI patients that receive TP (an observation not seen in the NBI patients) support the notion that TBI augments the systemic response following injury. We conclude that the combination of polytrauma (as observed in the E2 patients) with TBI results in a TP-responsive phenotype that processes allogeneic plasma differently than other severely injured patient groups. In addition, we identified the brain-specific biomarker UCHL1 as a predictive biomarker for E2-TBI patients. This differentiates UCHL1 from other brain injury biomarkers such as GFAP that only differentiates patients with or without TBI. Further research is required to identify the injury-specific mechanisms of the beneficial effects of early TP and whether UCHL1 could be used as a point-of-care biomarker to guide the treatment in the field.

Plasma multi-omics at 72 h revealed major differences between patients destined to resolve early and those patients defined as non-resolvers. Multiple cytokines, chemokines, and acute-phase proteins were selectively elevated at 72 h in the slow resolvers. Whether these patterns reflect an adaptation in patients that remain ill or are instead part of persistent pathogenic processes requires further investigation. We also found many molecules elevated in patients on their way to recovery, including lyso-phospholipids, sphingolipids, and complement components. These metabolites and proteins may be part of repair pathways and could serve as biomarkers for recovery.[46]

Limitations of study

There are several limitations to our study. Although we identify significant changes in many classes of circulating biomolecules that correlate with outcomes and treatment, our findings cannot establish causality. This will require mechanistic research in representative perturbation models. Confirmation of some of the notable changes in the metabolomics will require confirmation using quantitative assays. Finally, most of the measurement platforms were targeted assays; therefore, our analysis cannot be considered a complete description of all the changes in circulating proteins, lipids, or metabolites that take place after severe injury in humans.

STAR★METHODS

Detailed methods are provided in the online version of this paper and include the following:

- KEY RESOURCES TABLE
- RESOURCE AVAILABILITY
  - Lead contact
  - Materials availability
  - Data and code availability
- EXPERIMENTAL MODEL AND SUBJECT DETAILS
  - Patient and healthy volunteer enrollment
- METHOD DETAILS
  - Untargeted metabolomics assay
  - Quality control of metabolome data
  - Multiplexed proteomics assay
  - Quality control of proteome data
  - Targeted metabolites assay
  - Targeted proteins (biomarkers) assay
- QUANTIFICATION AND STATISTICAL ANALYSIS
  - Normalization, transformation and scaling
  - Dimension reduction and visualization
  - Unsupervised clustering
  - Metabolites family preference analysis
  - Pathway enrichment analysis
  - Feature selection and regression analysis
  - Predictive model for early stratification

Figure 7. Prehospital TP selectively benefits endotype 2-traumatic brain injury (E2-TBI) patients by targeting early massive consumption pattern

(A) Heatmap showing K-means clustering (k = 2) in trauma patients (n = 173) using 0 h data from three layers (Luminex, subsets 1–3; EC and metabolomics, modules 3 and 4).

(B) Kaplan-Meier curves for 30-day mortality showing patients grouped by endotype 1 (E1; n = 91) and E2 (n = 82). The p value was calculated by log rank test.

(C and D) Treatment effect of plasma for 30-day mortality for subgroups separated by E1 (C) or E2 (D) and with (TBI) or without (NBI) TBI and with or without prehospital TP. The p value was calculated by log rank test.

(E) Heatmap shows 41 proteins detected by proteomics differentially represented in patients based on the presence or absence of TBI and with or without prehospital TP at 0 and 24 h. Number of patients in each subgroup: 44 (NBI standard 0 h), 20 (TBI standard 0 h), 52 (NBI plasma 0 h), 24 (TBI plasma 24 h), 41 (NBI standard 24 h), 23 (TBI standard 0 h), 51 (NBI plasma 0 h), 24 (TBI plasma 24 h). *$p < 0.05$ for significant difference between treatment arms of TBI patients. #, $p < 0.05$ for significant difference between arms of NBI patients. The p value was calculated by K-W test.

(F) Diagram for a proposed mechanism for the selective effect of prehospital TP on the survival of E2-TBI patients.

- Generation of customized signature scores
- Survival, Correlation and Statistical analysis

SUPPLEMENTAL INFORMATION

Supplemental information can be found online at https://doi.org/10.1016/j.xcrm.2021.100478.

ACKNOWLEDGMENTS

This work was supported by US Army Medical Research and Materiel Command (W81XWH-12-2-0023 to J.L.S.) and National Institutes of Health (R35-GM-127027 to T.R.B.; R35GM119526 and R01HL141080 to M.D.N.; UM1HL120877 to J.H.M. and S.R.W. with sub-award to M.D.N.). We acknowledge the contribution of collaborators involved in PAMPer study for the clinical data collection. We acknowledge the contribution of the TACTIC team for proteomic data collection. J.W. was supported by Xiangya Medical School, Changsha, China.

AUTHOR CONTRIBUTIONS

Conceptualization, J.W. and T.R.B.; methodology, J.W., Y.V., and D.J.G.; software, J.W.; validation, J.W., S.A., and R.A.N.; formal analysis, J.W., S.A., N.K., R.G.V., and I.M.B.; investigation, J.W., D.S.G., A.C., P.I.J., J.S., and D.O.O.; resources, J.L.S., F.X.G., M.D.N., J.H.M., R.P.T., M.H.Y., B.J.D., R.S.M., B.G.H., J.A.C., H.A.P., S.R.W., B.S.Z., and T.R.B.; data curation, J.W., J.L.S., and R.A.N.; writing – original draft, J.W. and T.R.B.; writing – review & editing, J.W., Y.V., S.A., F.X.G., M.B.Y., D.O.O., M.D.N., J.L.S., and T.R.B.; visualization, J.W.; supervision, Y.V., M.D.N., J.L.S., and T.R.B.; project administration, J.W., U.K.K., J.H.M., M.D.N., J.L.S., and T.R.B.; funding acquisition, M.D.N., J.L.S., and T.R.B.

DECLARATION OF INTERESTS

Y.V. is co-founder and a stakeholder in Immunetrics. H.A.P. is a consultant for Avita Medical and Spectral MD. M.D.N. holds an equity stake in Haima Therapeutics. He has received research support and/or honoraria from Haemonetics, Instrumentation Laboratories, and Janssen Pharmaceuticals. T.R.B. is a stakeholder in Immunetrics. Other authors declare no conflict of interests.

Received: February 22, 2021
Revised: August 18, 2021
Accepted: November 23, 2021
Published: December 21, 2021

REFERENCES

1. GBD 2019 Diseases and Injuries Collaborators (2020). Global burden of 369 diseases and injuries in 204 countries and territories, 1990-2019: a systematic analysis for the Global Burden of Disease Study 2019. Lancet *396*, 1204–1222.
2. Maier, R.V. (2014). Scudder Oration on Trauma. A century of evolution in trauma resuscitation. J. Am. Coll. Surg. *219*, 335–345.
3. Dimopoulou, I., Tsagarakis, S., Theodorakopoulou, M., Douka, E., Zervou, M., Kouyialis, A.T., Thalassinos, N., and Roussos, C. (2004). Endocrine abnormalities in critical care patients with moderate-to-severe head trauma: incidence, pattern and predisposing factors. Intensive Care Med. *30*, 1051–1057.
4. Johansson, P.I., Stensballe, J., and Ostrowski, S.R. (2017). Shock induced endotheliopathy (SHINE) in acute critical illness - a unifying pathophysiologic mechanism. Crit. Care *21*, 25.
5. Neal, M.D., Moore, H.B., Moore, E.E., Freeman, K., Cohen, M.J., Sperry, J.L., Zuckerbraun, B.S., and Park, M.S.; TACTIC Investigators (2015). Clinical assessment of trauma-induced coagulopathy and its contribution to postinjury mortality: A TACTIC proposal. J. Trauma Acute Care Surg. *79*, 490–492.
6. Porter, C., Tompkins, R.G., Finnerty, C.C., Sidossis, L.S., Suman, O.E., and Herndon, D.N. (2016). The metabolic stress response to burn trauma: current understanding and therapies. Lancet *388*, 1417–1426.
7. Namas, R.A., Vodovotz, Y., Almahmoud, K., Abdul-Malak, O., Zaaqoq, A., Namas, R., Mi, Q., Barclay, D., Zuckerbraun, B., Peitzman, A.B., et al. (2016). Temporal patterns of circulating inflammation biomarker networks differentiate susceptibility to nosocomial infection following blunt trauma in humans. Ann. Surg. *263*, 191–198.
8. Xiao, W., Mindrinos, M.N., Seok, J., Cuschieri, J., Cuenca, A.G., Gao, H., Hayden, D.L., Hennessy, L., Moore, E.E., Minei, J.P., et al.; Inflammation and Host Response to Injury Large-Scale Collaborative Research Program (2011). A genomic storm in critically injured humans. J. Exp. Med. *208*, 2581–2590.
9. Cannon, J.W. (2018). Hemorrhagic Shock. N. Engl. J. Med. *378*, 370–379.
10. Cuenca, A.G., Gentile, L.F., Lopez, M.C., Ungaro, R., Liu, H., Xiao, W., Seok, J., Mindrinos, M.N., Ang, D., Baslanti, T.O., et al.; Inflammation and Host Response to Injury Collaborative Research Program (2013). Development of a genomic metric that can be rapidly used to predict clinical outcome in severely injured trauma patients. Crit. Care Med. *41*, 1175–1185.
11. Tompkins, R.G. (2015). Genomics of injury: The Glue Grant experience. J. Trauma Acute Care Surg. *78*, 671–686.
12. Shilo, S., Rossman, H., and Segal, E. (2020). Axes of a revolution: challenges and promises of big data in healthcare. Nat. Med. *26*, 29–38.
13. Wozniak, J.M., Mills, R.H., Olson, J., Caldera, J.R., Sepich-Poore, G.D., Carrillo-Terrazas, M., Tsai, C.-M., Vargas, F., Knight, R., Dorrestein, P.C., et al. (2020). Mortality Risk Profiling of Staphylococcus aureus Bacteremia by Multi-omic Serum Analysis Reveals Early Predictive and Pathogenic Signatures. Cell *182*, 1311–1327.e14.
14. Reyes, M., Filbin, M.R., Bhattacharyya, R.P., Billman, K., Eisenhaure, T., Hung, D.T., Levy, B.D., Baron, R.M., Blainey, P.C., Goldberg, M.B., and Hacohen, N. (2020). An immune-cell signature of bacterial sepsis. Nat. Med. *26*, 333–340.
15. Arunachalam, P.S., Wimmers, F., Mok, C.K.P., Perera, R.A.P.M., Scott, M., Hagan, T., Sigal, N., Feng, Y., Bristow, L., Tak-Yin Tsang, O., et al. (2020). Systems biological assessment of immunity to mild versus severe COVID-19 infection in humans. Science *369*, 1210–1220.
16. Shen, B., Yi, X., Sun, Y., Bi, X., Du, J., Zhang, C., Quan, S., Zhang, F., Sun, R., Qian, L., et al. (2020). Proteomic and Metabolomic Characterization of COVID-19 Patient Sera. Cell *182*, 59–72.e15.
17. Chen, T., Delano, M.J., Chen, K., Sperry, J.L., Namas, R.A., Lamparello, A.J., Deng, M., Conroy, J., Moldawer, L.L., Efron, P.A., et al. (2020). A roadmap from single-cell transcriptome to patient classification for the immune response to trauma. JCI Insight *6*, e145108.
18. Zhang, Q., Bastard, P., Liu, Z., Le Pen, J., Moncada-Velez, M., Chen, J., Ogishi, M., Sabli, I.K.D., Hodeib, S., Korol, C., et al.; COVID-STORM Clinicians; COVID Clinicians; Imagine COVID Group; French COVID Cohort Study Group; CoV-Contact Cohort; Amsterdam UMC Covid-19 Biobank; COVID Human Genetic Effort; NIAID-USUHS/TAGC COVID Immunity Group (2020). Inborn errors of type I IFN immunity in patients with life-threatening COVID-19. Science *370*, 370.
19. van der Poll, T., van de Veerdonk, F.L., Scicluna, B.P., and Netea, M.G. (2017). The immunopathology of sepsis and potential therapeutic targets. Nat. Rev. Immunol. *17*, 407–420.
20. Wiersinga, W.J., Rhodes, A., Cheng, A.C., Peacock, S.J., and Prescott, H.C. (2020). Pathophysiology, Transmission, Diagnosis, and Treatment of Coronavirus Disease 2019 (COVID-19): A Review. JAMA *324*, 782–793.
21. Sperry, J.L., Guyette, F.X., Brown, J.B., Yazer, M.H., Triulzi, D.J., Early-Young, B.J., Adams, P.W., Daley, B.J., Miller, R.S., Harbrecht, B.G., et al.; PAMPer Study Group (2018). Prehospital Plasma during Air Medical Transport in Trauma Patients at Risk for Hemorrhagic Shock. N. Engl. J. Med. *379*, 315–326.
22. Gruen, D.S., Brown, J.B., Guyette, F.X., Vodovotz, Y., Johansson, P.I., Stensballe, J., Barclay, D.A., Yin, J., Daley, B.J., Miller, R.S., et al.; PAMPer

study group (2020). Prehospital plasma is associated with distinct biomarker expression following injury. JCI Insight *5*, e135350.

23. Wu, J., Cyr, A., Gruen, D., Lovelace, T., Benos, P., Chen, T., Guyette, F., Yazer, M., Daley, B., Miller, R., et al. (2021). Lipidomic Signatures Align with Inflammatory Patterns and Outcomes in Critical Illness. Res Sq rs.3.rs-106579. https://doi.org/10.21203/rs.3.rs-106579/v1.
24. Cyr, A., Zhong, Y., Reis, S.E., Namas, R.A., Amoscato, A., Zuckerbraun, B., Sperry, J., Zamora, R., Vodovotz, Y., and Billiar, T.R. (2021). Analysis of the Plasma Metabolome after Trauma, Novel Circulating Sphingolipid Signatures, and In-Hospital Outcomes. J. Am. Coll. Surg. *232*, 276–287.e1.
25. McInnes, L., Healy, J., and Melville, J. (2018). Umap: Uniform manifold approximation and projection for dimension reduction. arXiv, 1802.03426. https://arxiv.org/abs/1802.03426.
26. Chen, R., Kang, R., Fan, X.G., and Tang, D. (2014). Release and activity of histone in diseases. Cell Death Dis. *5*, e1370.
27. Böhmer, A.B., Wappler, F., and Zwissler, B. (2014). Preoperative risk assessment–from routine tests to individualized investigation. Dtsch. Arztebl. Int. *111*, 437–445, quiz 446.
28. Gruen, D.S., Guyette, F.X., Brown, J.B., Okonkwo, D.O., Puccio, A.M., Campwala, I.K., Tessmer, M.T., Daley, B.J., Miller, R.S., Harbrecht, B.G., et al. (2020). Association of prehospital plasma with survival in patients with traumatic brain injury: A secondary analysis of the pamper cluster randomized clinical trial. JAMA Netw. Open *3*, e2016869.
29. Timmermans, K., Kox, M., Vaneker, M., van den Berg, M., John, A., van Laarhoven, A., van der Hoeven, H., Scheffer, G.J., and Pickkers, P. (2016). Plasma levels of danger-associated molecular patterns are associated with immune suppression in trauma patients. Intensive Care Med. *42*, 551–561.
30. Cohen, M.J., Brohi, K., Calfee, C.S., Rahn, P., Chesebro, B.B., Christiaans, S.C., Carles, M., Howard, M., and Pittet, J.-F. (2009). Early release of high mobility group box nuclear protein 1 after severe trauma in humans: role of injury severity and tissue hypoperfusion. Crit. Care *13*, R174.
31. Zhang, Q., Raoof, M., Chen, Y., Sumi, Y., Sursal, T., Junger, W., Brohi, K., Itagaki, K., and Hauser, C.J. (2010). Circulating mitochondrial DAMPs cause inflammatory responses to injury. Nature *464*, 104–107.
32. Abrams, S.T., Zhang, N., Manson, J., Liu, T., Dart, C., Baluwa, F., Wang, S.S., Brohi, K., Kipar, A., Yu, W., et al. (2013). Circulating histones are mediators of trauma-associated lung injury. Am. J. Respir. Crit. Care Med. *187*, 160–169.
33. Yang, R., Harada, T., Mollen, K.P., Prince, J.M., Levy, R.M., Englert, J.A., Gallowitsch-Puerta, M., Yang, L., Yang, H., Tracey, K.J., et al. (2006). Anti-HMGB1 neutralizing antibody ameliorates gut barrier dysfunction and improves survival after hemorrhagic shock. Mol. Med. *12*, 105–114.
34. Johansson, P.I., Stensballe, J., Rasmussen, L.S., and Ostrowski, S.R. (2011). A high admission syndecan-1 level, a marker of endothelial glycocalyx degradation, is associated with inflammation, protein C depletion, fibrinolysis, and increased mortality in trauma patients. Ann. Surg. *254*, 194–200.
35. Almahmoud, K., Namas, R.A., Zaaqoq, A.M., Abdul-Malak, O., Namas, R., Zamora, R., Sperry, J., Billiar, T.R., and Vodovotz, Y. (2015). Prehospital hypotension is associated with altered inflammation dynamics and worse outcomes following blunt trauma in humans. Crit. Care Med. *43*, 1395–1404.
36. Régnier, M.-A., Raux, M., Le Manach, Y., Asencio, Y., Gaillard, J., Devilliers, C., Langeron, O., and Riou, B. (2012). Prognostic significance of blood lactate and lactate clearance in trauma patients. Anesthesiology *117*, 1276–1288.
37. Huber-Lang, M., Lambris, J.D., and Ward, P.A. (2018). Innate immune responses to trauma. Nat. Immunol. *19*, 327–341.
38. Namas, R.A., Mi, Q., Namas, R., Almahmoud, K., Zaaqoq, A.M., Abdul-Malak, O., Azhar, N., Day, J., Abboud, A., Zamora, R., et al. (2015). Insights into the Role of Chemokines, Damage-Associated Molecular Patterns, and Lymphocyte-Derived Mediators from Computational Models of Trauma-Induced Inflammation. Antioxid. Redox Signal. *23*, 1370–1387.
39. Chang, R., Cardenas, J.C., Wade, C.E., and Holcomb, J.B. (2016). Advances in the understanding of trauma-induced coagulopathy. Blood *128*, 1043–1049.
40. Zhang, J., Zhang, F., and Dong, J.-F. (2018). Coagulopathy induced by traumatic brain injury: systemic manifestation of a localized injury. Blood *131*, 2001–2006.
41. Moore, H.B., Gando, S., Iba, T., Kim, P.Y., Yeh, C.H., Brohi, K., Hunt, B.J., Levy, J.H., Draxler, D.F., Stanworth, S., et al.; Subcommittees on Fibrinolysis, Disseminated Intravascular Coagulation, and Perioperative and Critical Care Thrombosis and Hemostasis (2020). Defining trauma-induced coagulopathy with respect to future implications for patient management: Communication from the SSC of the ISTH. J. Thromb. Haemost. *18*, 740–747.
42. Foley, J.H. (2016). Examining coagulation-complement crosstalk: complement activation and thrombosis. Thromb. Res. *141* (*Suppl 2*), S50–S54.
43. Huber-Lang, M., Kovtun, A., and Ignatius, A. (2013). The role of complement in trauma and fracture healing. Semin. Immunol. *25*, 73–78.
44. Keragala, C.B., Draxler, D.F., McQuilten, Z.K., and Medcalf, R.L. (2018). Haemostasis and innate immunity - a complementary relationship: A review of the intricate relationship between coagulation and complement pathways. Br. J. Haematol. *180*, 782–798.
45. Jackson, S.P., Darbousset, R., and Schoenwaelder, S.M. (2019). Thromboinflammation: challenges of therapeutically targeting coagulation and other host defense mechanisms. Blood *133*, 906–918.
46. Thorgersen, E.B., Barratt-Due, A., Haugaa, H., Harboe, M., Pischke, S.E., Nilsson, P.H., and Mollnes, T.E. (2019). The role of complement in liver injury, regeneration, and transplantation. Hepatology *70*, 725–736.
47. Shannon, P., Markiel, A., Ozier, O., Baliga, N.S., Wang, J.T., Ramage, D., Amin, N., Schwikowski, B., and Ideker, T. (2003). Cytoscape: a software environment for integrated models of biomolecular interaction networks. Genome Res. *13*, 2498–2504.
48. Yu, G., Wang, L.-G., Han, Y., and He, Q.-Y. (2012). clusterProfiler: an R package for comparing biological themes among gene clusters. OMICS *16*, 284–287.
49. Brock, G., Pihur, V., Datta, S., and Datta, S. (2011). clValid, an R package for cluster validation. J. Stat. Softw. *25*, 1–22.
50. Candia, J., Cheung, F., Kotliarov, Y., Fantoni, G., Sellers, B., Griesman, T., Huang, J., Stuccio, S., Zingone, A., Ryan, B.M., et al. (2017). Assessment of variability in the somascan assay. Sci. Rep. *7*, 14248.
51. Davies, D.R., Gelinas, A.D., Zhang, C., Rohloff, J.C., Carter, J.D., O'Connell, D., Waugh, S.M., Wolk, S.K., Mayfield, W.S., Burgin, A.B., et al. (2012). Unique motifs and hydrophobic interactions shape the binding of modified DNA ligands to protein targets. Proc. Natl. Acad. Sci. USA *109*, 19971–19976.
52. Zhang, L., Yu, X., Zheng, L., Zhang, Y., Li, Y., Fang, Q., Gao, R., Kang, B., Zhang, Q., Huang, J.Y., et al. (2018). Lineage tracking reveals dynamic relationships of T cells in colorectal cancer. Nature *564*, 268–272.
53. Bazarian, J.J., Biberthaler, P., Welch, R.D., Lewis, L.M., Barzo, P., Bogner-Flatz, V., Gunnar Brolinson, P., Büki, A., Chen, J.Y., Christenson, R.H., et al. (2018). Serum GFAP and UCH-L1 for prediction of absence of intracranial injuries on head CT (ALERT-TBI): a multicentre observational study. Lancet Neurol. *17*, 782–789.
54. Ackerman, M.E., Das, J., Pittala, S., Broge, T., Linde, C., Suscovich, T.J., Brown, E.P., Bradley, T., Natarajan, H., Lin, S., et al. (2018). Route of immunization defines multiple mechanisms of vaccine-mediated protection against SIV. Nat. Med. *24*, 1590–1598.

STAR★METHODS

KEY RESOURCES TABLE

REAGENT or RESOURCE	SOURCE	IDENTIFIER
Biological samples		
Plasma samples from patients enrolled in PAMPer Trial and healthy volunteers	Sperry et al.[21]	N/A
Chemicals, peptides, and recombinant proteins		
Human CD138 ELISA Kit	Nordic Biosite	Cat# 950.640.192
Human CD141 ELISA Kit	Nordic Biosite	Cat# 850.720.192
Human VEGFR1/Flt-1 Quantikine ELISA Kit	Bio-Techne	Cat# DVR100C
Cell Death Detection ELISA^{PLUS}	Roche	Cat# 11774425001
suPARnostic® ELISA assay	ViroGates	Cat# E001
Human S100 Calcium-binding Protein A10 (S100A10) ELISA Kit	Abbexa	Cat# abx152996
Human Total Adiponectin/Acrp30 Quantikine ELISA	Bio-Techne	Cat# DPR300
MILLIPLEX MAP Human Cytokine/ Chemokine Magnetic Bead Panel	Millipore	Cat# HCYTOMAG-60K
MILLIPLEX MAP Human TH17 Magnetic Bead Panel	Millipore	Cat# HTH17MAG-14K
MILLIPLEX MAP Human Cytokine/ Chemokine Magnetic Bead Panel III	Millipore	Cat# HCYP3MAG-63K
Banyan UCH-L1 Kit	Banyan Biomarkers	Cat# BC-1208
Banyan GFAP Kit	Banyan Biomarkers	Cat# BC-1210
Critical commercial assays		
SOMAscan® 1.3k assay	somaLogic	N/A
Metabolomics LC-MS global metabolomics	Metabolon	N/A
Deposited data		
[Database]: [PAMPer Trial Metabolomics and Proteomics Dataset]	This study	https://doi.org/10.17632/vt8nhp2y2t.1
Software and algorithms		
R, v3.6.0	R Project	https://www.r-project.org
Cytoscape, v3.8.0	Markiel et al.[47]	https://cytoscape.org
ggplot2, v3.0.0	RStudio	https://cran.r-project.org/web/packages/ggplot2/index.html
clusterProfiler, v3.11	Yu et al.[48]	https://bioconductor.org/packages/release/bioc/html/clusterProfiler.html
survival, v2.43.3	Therneau et al.	https://cran.r-project.org/web/packages/survival/index.html
clValid	Brock et al.[49]	https://cran.r-project.org/web/packages/clValid/index.html
Caret, v6.0-86	Kuhn et al.	https://cran.r-project.org/web/packages/caret/index.html
Analysis codes	This study	https://github.com/Junru-max/PAMPer-Multi-omic-analysis

RESOURCE AVAILABILITY

Lead contact

Further information and requests for resources and reagents should be directed to and will be fulfilled by the Lead Contact, Timothy R. Billiar (billiartr@upmc.edu).

CellPress
OPEN ACCESS

Materials availability

This study did not generate new unique reagents.

Data and code availability

The proteomics and metabolomics data generated by this study are available at Mendeley Data https://doi.org/10.17632/vt8nhp2y2t.1. Code supporting the current study is deposited at https://github.com/Junru-max/PAMPer-Multi-omic-analysis. Any additional information required to reanalyze the data reported in this work paper is available from the Lead Contact upon request.

EXPERIMENTAL MODEL AND SUBJECT DETAILS

Patient and healthy volunteer enrollment

We conducted analyses of plasma samples obtained at three time point (0, 24 and 72 h) for 194 and 156 patients in metabolome and proteome layers, respectively, enrolled in the PAMPer Trial.[21] Only the first time point was available for patients that died in the first 72 h. 17 non-fasting healthy volunteers were also analyzed with the patients in the metabolome layer. Enrollment criteria and patient characteristics have been previously reported (Sperry et al., 2018). Briefly, patients were enrolled by air ambulance crews that had experienced at least one episode of hypotension (systolic blood pressure < 90 mm Hg) and tachycardia (defined in this trial as a heart rate > 108 beats per minute) or if they had any severe hypotension (systolic blood pressure < 70 mm Hg). Patients were excluded if they experienced burns over 20% body surface, penetrating brain injury or cardiac arrest lasting over 5 min. Patients were randomized into arms of TP (prehospital administration of two units of allogeneic TP followed by standard fluid resuscitation) or standard of care (standard fluid, crystalloid or crystalloid and packed RBC).

The order for the measurement of each data layer was cytokines, EC biomarkers, lipidome, metabolome to proteome. The patient and sample selection for the EC, cytokine and lipidome data layers were previously reported.[22,23] Briefly, patients with available samples from the PAMPer trial (n = 405) were utilized for the (Plasma arm: 188, Standard arm: 217) in cytokine and EC biomarker layers. Patients with samples but with missing data were excluded for both EC (n = 15) and cytokines layers (n = 12), yielding 393 and 390 patients, respectively. Following the analyses of the cytokine and EC biomarkers samples for 293 patients remained. For the remainder of the analyses, we selected all of the nonsurvivors (n = 83), all the surviving TBI patients (n = 58), and then randomly selected surviving NBI patients (n = 53) yielding a total of 194 patients. Patients selected for the proteome layer overlapped with lipidome and metabolome data layers patients except that only 5 early-nonsurviors were included. A total of 59 resolving and 92 non-resolving patients were included in this layer (Total n = 151).

The information in the clinical, cytokine, EC biomarkers and lipidome data layers were reported previously.[21–23] EDTA plasma samples were collected and stored at −80°C for further analysis. The TD-2 dataset only enrolled patients expected to survive from blunt trauma and all three layers were reported previously (Cyr et al., 2021).

This study was approved by the IRB of University of Pittsburgh. Detailed information and study protocol for PAMPer Trial are avaible on https://clinicaltrials.gov/ct2/show/NCT01818427. The PAMPer Trial received approval for Emergency Exception from Informed Consent (EFIC) protocol from the Human Research Protection Office of the US Army Medical Research and Material Command.

METHOD DETAILS

Untargeted metabolomics assay

The same UPLC-MS/MS platform was used for the untargeted metabolomic assay for PAMPer Trial and the TD-2 dataset. 500ul of EDTA- treated plasma was aliquoted and sent on dry ice to Metabolon Inc. (Durham, NC, US) for metabolite measurement. Several recovery standards were added prior to the first step in the extraction process for QC purposes. Proteins were precipitated with methanol under vigorous shaking for 2 min (Glen Mills GenoGrinder 2000) followed by centrifugation. The resulting extract was divided into five fractions: two for analysis by two separate reverse phases (RP)/UPLC-MS/MS methods with positive ion mode electrospray ionization (ESI), one for analysis by RP/UPLC-MS/MS with negative ion mode ESI, one for analysis by HILIC/UPLC-MS/MS with negative ion mode ESI, and one sample was reserved for backup. Samples were placed briefly on a TurboVap (Zymark) to remove the organic solvent. The sample extracts were stored overnight under nitrogen before preparation for analysis.

All methods utilized a Waters ACQUITY ultra-performance liquid chromatography (UPLC) and a Thermo Scientific Q-Exactive high resolution/accurate mass spectrometer interfaced with a heated electrospray ionization (HESI-II) source and Orbitrap mass analyzer operated at 35,000 mass resolution. The sample extract was dried then reconstituted in solvents compatible to each of the four methods. Each reconstitution solvent contained a series of standards at fixed concentrations to ensure injection and chromatographic consistency. One aliquot was analyzed using acidic positive ion conditions, chromatographically optimized for more hydrophilic compounds. In this method, the extract was gradient eluted from a C18 column (Waters UPLC BEH C18-2.1x100 mm, 1.7 μm) using water and methanol, containing 0.05% perfluoropentanoic acid (PFPA) and 0.1% formic acid (FA). Another aliquot was also analyzed using acidic positive ion conditions; however, it was chromatographically optimized for more hydrophobic compounds. In this method, the extract was gradient eluted from the same afore mentioned C18 column using methanol, acetonitrile, water, 0.05% PFPA and 0.01% FA and was operated at an overall higher organic content. Another aliquot was analyzed using basic negative ion optimized conditions

using a separate dedicated C18 column. The basic extracts were gradient eluted from the column using methanol and water, however with 6.5mM Ammonium Bicarbonate at pH 8. The fourth aliquot was analyzed via negative ionization following elution from a HILIC column (Waters UPLC BEH Amide 2.1x150 mm, 1.7 μm) using a gradient consisting of water and acetonitrile with 10mM Ammonium Formate, pH 10.8. The MS analysis alternated between MS and data-dependent MSn scans using dynamic exclusion. The scan range varied slighted between methods but covered 70-1000 m/z.

Raw data was extracted, peak-identified and QC processed using in-house software and library of over 3300 commercially available purified standard compounds. Compounds were identified by comparison to library entries of purified standards or recurrent unknown entities. Furthermore, biochemical identifications are based on three criteria: retention index within a narrow RI window of the proposed identification, accurate mass match to the library ± 10 ppm, and the MS/MS forward and reverse scores between the experimental data and authentic standards. The MS/MS scores are based on a comparison of the ions present in the experimental spectrum to the ions present in the library spectrum. Additional mass spectral entries have been created for structurally unnamed biochemicals, which have been identified by virtue of their recurrent nature (both chromatographic and mass spectral).

Quality control of metabolome data

Several types of controls were analyzed in concert with the experimental samples: a pooled matrix sample generated by taking a small volume of each experimental sample served as a technical replicate throughout the dataset; extracted water samples served as process blanks; and a cocktail of QC standards that were carefully chosen not to interfere with the measurement of endogenous compounds were spiked into every analyzed sample, allowed instrument performance monitoring and aided chromatographic alignment. Instrument variability was determined by calculating the median relative standard deviation (RSD) for the standards that were added to each sample prior to injection into the mass spectrometers. Overall process variability was determined by calculating the median RSD for all endogenous metabolites (i.e., non-instrument standards) present in 100% of the pooled matrix samples. The Median RSD for the Internal Standards and Endogenous Biochemicals are 4% and 9% respectively in the metabolome layer of PAMPer Trial.

Multiplexed proteomics assay

We adopted a multiplexed, aptamer-based approach (SOMAscan assay) capable of measuring 1,305 human proteins in plasma.[50] The full lists of protein names, Entrez gene symbol, Entrez ID, Uniprot ID was shown in Table S5. 150 μL of EDTA-treated plasma was aliquoted and sent on dry ice to SomaLogic Inc. (Boulder, Colorado, US) for protein measurement. The technical details for the SOMAscan assay can be found in Technical White Paper. Briefly, the assay is based on a protein-capture SOMAmer reagents which are constructed with chemically modified single stranded DNA. The SOMAmer mimic amino acid side chains and can specifically bind to the targeted proteins. The specific interaction between SOMAmer and targeted proteins shows a similar structure compared to antibody-antigen interaction.[51] The proteins relative concentration is positive correlated to the intensity of SOMAmer which can be detected using a DNA microarray.

Quality control of proteome data

Two types of quality control (Hybridization and Calibration) were conducted to evaluate the variability at the level of samples and experiments for the SOMAscan assay. Hybridization by adding the control probes (part of the SOMAmer reagent) was used to evaluate the bias caused by differential readout conditions (eluate, transfer, hybridization, wash, scan) in individual microarrays. A scaled factor for each sample was calculated based on the hybridization control. Calibration is accomplished using a number of replicate measurements of a common pooled calibrator sample which was used to correct run-to-run (plate-to-plate) variation. A unique calibration scale factor is derived for each SOMAmer binding reagent within the assay and then applied to all SOMAmer measurements within the set of samples in that run (plate). The accepted range for the Hybridization and Calibration Scale factors are 0.4-2.5 and 0.8-1.2 respectively. The median normalization for the variability related to the protein concentration was not applied in this study due to the expectation of a dramatic alteration of concentration post trauma.

Targeted metabolites assay

Samples from 10 healthy subjects and 10 early nonsurvivors from PAMPer (5 TP and 5 standard care) were analyzed for TCA cycle metabolites in The University of Pittsburgh Health Sciences Metabolomics and Lipidomics Core. Metabolic quenching, polar metabolite pool extraction, and internal standardization were performed prior to detection. Calibration curves were prepared and derivatized identically for malate, succinate, pyruvate, citrate, oxaloaceteate, fumarate, alphaketoglutarate, and cisaconitate using serial dilution. All analyte peak areas were normalized to (D6)-propionate and expressed as the ration of peak area to internal standard before concentration conversion. Analyses were performed by liquid chromatography-high resolution mass spectrometry. Samples were injected via a Thermo Vanquish UHPLC and separated over a reversed phase Phenomenex Kinetex C18 column (2.1 × 150mm, 1.7 μm particle size) maintained at 55°C. The Thermo IDX tribrid mass spectrometer was operated in negative mode, scanning in Full MS mode. Calibration was performed prior to analysis using the PierceTM FlexMix Ion Calibration Solutions (Thermo Fisher Scientific). Integrated peak areas were then extracted manually using Quan Browser (Thermo Fisher Xcalibur ver. 2.7).

CellPress
OPEN ACCESS

Targeted proteins (biomarkers) assay

Details for the quantitive measurement of 21 cytokines, 7 EC biomarkers, and 2 brain injury related biomarkers were reported previously.[22,28] Briefly, inflammatory mediators were measured using three kits from Luminex assay MAGPIX (Austin, TX, Luminex Inc). The Luminex system was used in accordance to manufacturer's instructions. EC biomarkers were assayed by commercially available immunoassays (ELISA) separately. Quantitative value as concentration for all 21 cytokines and 7 EC biomarkers (except for HCDNA) were recorded. Concentration of 2 brain injury related biomarkers UCHL1 and GFAP were detected using chemiluminescent enzyme-linked immunosorbent assays.

QUANTIFICATION AND STATISTICAL ANALYSIS

Normalization, transformation and scaling

Missing data were evaluated in each layer and the variables with over 20% missing were removed. The median value was used to infer the missing data clinical layer due to the possibility of unrecording. Minimum value was used to infer the missing data from cytokines and EC layer due to the possibility of detection limit. For untargeted metabolomics layer, raw peak intensity data were normalized by a median normalization to equal one (1.00) based on the run-day blocks for each metabolite. For Multiplexed proteomics, raw fluorescent intensity data were normalized by multiple Hybridization and Calibration Scale factors for each sample respectively. The normalized data for each layer were further log2 transformed to obey a normal distribution approximately. The log2 transformed data were auto-scaled (Z score) across each sample for downstream analysis for different purpose (e.g., Visualization in heatmap, Dimension reduction).

Dimension reduction and visualization

Two-step dimension reduction (Linear & Nonlinear) was applied for exploration of global patterns. First, the principal component analysis was conducted in the normalized data for each layer (except for the clinical layer). The PC numbers were set as 20 and 15 for metabolomics and proteomics, respectively. Second, the top 15 and 10 PCs were selected (> 95% variance explained) for UMAP analysis,[25] which is a non-linear method for dimension reduction and more sensitive than linear methods to the subtle differences. The visualization for the UMAP dimension reduction is based on a scatterplot. Each dot represents one sample and was labeled with outcome, time point or injury severity according to the purpose.

Unsupervised clustering

Two types of unsupervised clustering method were used in this study. The first was Hierarchical clustering which was conducted based on the ''Euclidean distance'' and the exact method was set as ''complete.'' The second was consensus K-means clustering repeated 1000 times. The choice and validation for numbers of clusters was performed in R package clValid.[49] The suitable numbers of K were evaluated by two types of measures together with reasonable biological interpretation. Internal measures include the connectivity, and Silhouette Width, and Dunn Index were used to evaluate the connectedness, compactness and separation of the clusters. External measures include the average proportion of non-overlap (APN), the average distance (AD), the average distance between means (ADM), and the figure of merit (FOM) were used to evaluate the stability of the k-means clustering result. The evaluation results of metabolites clustering in PAMPer dataset for three methods (Hierarchical, K-means, Partitioning Around Medoids: PAM) can be found in Figures S4A and S4B. The dendrogram for the clustering results were diminished for some heatmaps for visualization.

Metabolites family preference analysis

The method for metabolites family preference analysis was modified from previous reports.[52] A constancy table of metabolite families by the seven modules we identified in Figure 3C and chi-square tested was applied to evaluate whether different metabolite families were randomly distributed in each module. We then computed the Ro/e for each combination of metabolite family according to the follow formula:

$$\text{Ro}/\text{e} = \text{observed number of metabolites}/\text{expected number of metabolites}$$

Where Ro/e is the ratio of observed metabolites number over the expected metabolites of a given combination of metabolite families and modules. The Ro/e can reflect whether a metabolites family is enriched in the module or not. For instance, if the Ro/e > 1, this suggests that the metabolite family is enriched in that module more than other modules. If the Ro/e < 1, this suggests that the metabolite family is depleted in that module compared to other modules.

Pathway enrichment analysis

Over-representation method was applied for pathway enrichment analysis in R package Clusterprofiler (v 3.1148). Names of 880 up-regulated proteins ($p < 0.05$ & Fold change > 1.2) at 0 h were transformed into Entrez ID and database of Reactome was used to search related pathways. The P value of enriched pathways was adjusted by BH method. Pathways with adjusted P value < 0.05 were consider to be significant.

Feature selection and regression analysis

Five statistical/machine learning methods (ROC Curve, logistical regression with lasso regularization, logistical regression with elastic-net regularization, SIMPLS algorithm from partial least-squares regression, random forest) were applied to evaluate the predictive value of variables in each layer for binary outcome (early-death, non-resolving pattern). R package Caret was used to tune the parameters with 10-fold cross-validation. A score from 0-100 was computed by all five methods to each variable to evaluate the relative contribution. Top 25 metabolites/proteins were visualized and ranked by average score from the five methods.

Logistical regression with elastic-net regularization was applied to predict the binary outcome (early-death, non-resolving pattern, clinical coagulopathy). The combination of elastic net mixing parameter(alpha) and penalty(lambda) was tuned by 10 different values with 10-fold cross-validation. Multi-variable Cox regression modeling was applied to the survival data (Time to death).

Predictive model for early stratification

173 patients labeled both TBI and endotype were included for the establishment of predictive model. Only quantitive biomarkers (2 brain-specific biomarkers, 21 cytokines and 7 EC injury related biomarkers) were included for the analysis. The 2 brain-specific biomarkers were missing in 9 TBI and 72 NBI patients, which was imputed by the median value for these. The imputed value of GFAP and UCHL1 were 33 pg/mL and 548.5pg/mL for NBI patients, which was close to a previous report.[53] A cut off of 22 pg/mL of GFAP and 327 pg/mL of UCHL1 (< 12 h) were used to identify mild TBI patients. For detection of intracranial injury, the test had a sensitivity of 0·976 (95% CI 0·931–0·995) and an NPV of 0·996 (0·987–0·999).[53]

The importance of biomarkers for early stratification were evaluated by a machine learning based two-step feature selection strategy as previously reported.[54] Briefly, two models (least absolute shrinkage and selection operator: lasso; support vector machine with the radial basis function: SVM-RBF) were fitted sequentially and 100 times repeated and nested 5-fold cross-validation (Both outer and inner sampling were 5 folds). The lasso model was fitted into inner sampling of each 5-fold for tuning the hyperparameter. Then a fold-specific classifier was trained by SVM-RBF in the selected features from the lasso model in the same fold. The performance (accuracy) of the fold-specific classifier was internally evaluated in the outer-sampling. The frequency of selected features was summarized in all models with accuracy > 0.8. The top selected features (UCHL1, Syndecan1, IP10, IL17A) were used for classification by logistical regression model with 10-fold cross-validation.

Generation of customized signature scores

Detailed definition and explanation about the customized signature scores can be found in Table S7. Briefly, a signature score to summarize major patterns in each layer was applied for downstream analysis (i.e., Correlation or Clustering). The signature score was more stable than individual variables and this might reflect the magnitude of a common biological process. Average *Z* score was used to generate the customized signature scores for selected metabolites/proteins sets.

Survival, Correlation and Statistical analysis

Survival analyses were conducted by K-M curve and raw log rank p values were computed. Spearman correlation analysis was applied to reveal the non-linear correlation among variables from different layers and p value was estimated by Spearman's rho statistic from Algorithm AS 89 with multiple test correction by FDR. Pearson's $\chi 2$ test or Kruskal-Wallis test was used for categorical variables or continuous variables in the contingency table of clinical layer data. Multiple group comparisons were conducted by Kruskal-Wallis test with post hoc analysis by Dunn test. Time-series analyses were tested by Two-way ANOVA with pairwise comparisons Estimated Marginal Means test. Differential metabolites/proteins were generated by Wilcoxon Rank Sum test and p value adjustment was performed using Bonferroni correction.